August 2020

Biennial and Low-Frequency Components of El Niño/Southern Oscillation

James Michael Ryan
University of Wisconsin-Milwaukee

BIENNIAL AND LOW-FREQUENCY COMPONENTS OF EL NIÑO/SOUTHERN OSCILLATION

by

James Ryan

A Thesis Submitted in

Partial Fulfillment of the

Requirements for the Degree of

Master of Science

in Atmospheric Science

at

The University of Wisconsin-Milwaukee

August 2020

ABSTRACT

BIENNIAL AND LOW-FREQUENCY COMPONENTS OF EL NIÑO/SOUTHERN OSCILLATION

by

James Ryan

The University of Wisconsin-Milwaukee, 2020
Under the Supervision of Professor Sergey Kravtsov

El Niño/Southern Oscillation (ENSO) is a coupled oscillation of sea surface temperatures (SSTs), winds, and air pressure in the eastern and central tropical Pacific, that repeats with quasi-regularity, every 2–7 years. Although the ENSO's spectral peak is found at a 4–7-yr period, composite El Niño events, taken as the 84 months before and after the peak of each El Niño, show that the length of each event, and often the following La Niña if there is one, usually falls within a quasi-biennial (QB) range of around 18–42 months. We argue that the biennial range of ENSO events stems from the classical delayed oscillator dynamics, while the lower-frequency range is from interaction with the extratropics; these interactions also lead to much of ENSO's irregularity.

After applying an 18–42 month bandpass filter to historical monthly temperature record and comparing filtered temperature variance to that of the raw temperature anomalies, the tropical Pacific emerges as the major center of enhanced ratio of biennial-to-total variance. This suggests that ENSO might be primarily driven by processes in this frequency band, even if its spectral peak is at lower frequencies. Discriminating patterns that maximize the ratio of biennial-to-total variance of surface temperatures also point to ENSO as the primary and only significant mode, both when projected onto monthly and bandpass-filtered surface temperature and SST

data. We also compare composites, power spectra, variance ratio maps and time series, and discriminating patterns from observations to some CMIP5 global climate models, many of which have ENSO be too regular, and/or attribute too much of ENSO's variability to the QB timescale. Finally, to put these ideas in a dynamical perspective, we investigate a coupled model that includes biennial tropical dynamics augmented by extratropical feedbacks, which shows much more LF and decadal variability reminiscent of the observed ENSO behavior.

TABLE OF CONTENTS

LIST OF FIGURES

ACKNOWLEDGEMENTS

Thank you to Dr. Kravtsov for providing the guidance needed to finish this project. He was quite receptive to questions, gave insightful feedback, and led me through many concepts I had little to no exposure to in my coursework.

Thank you to Dr. Evans and Dr. Roebber for serving on my committee alongside Dr. Kravtsov.

Finally, thank you to my friends and family for all the support with this project and everything else in life.

1. Introduction

El Niño-Southern Oscillation (ENSO) is the leading coupled mode of variability in the tropical Pacific ocean–atmosphere system, with anomalously warm events repeating every 2–7 years (Capotondi et al., 2015). El Niño was named by South American fishermen who sometimes noticed abnormally warm water in the equatorial Pacific, often around Christmas, so they named it after Jesus. The cool phase was later named La Niña. While El Niño refers to ocean surface temperatures, the Southern Oscillation is an atmospheric phenomenon. Sir Gilbert Walker found a connection between air pressure measurements on the island of Tahiti in the central Pacific, and Darwin, Australia, at the western edge of the Pacific, in 1910. Over half a century later, Jacob Bjerknes found a connection between the oceanic El Niño and the atmospheric Southern Oscillation, finding it to be a coupled phenomenon.

When wind weakens near South America, wind stress on surface water decreases, so less water needs to be replaced by cooler water from below. With less upwelling, SSTs increase in the tropical Pacific. This is a commonly agreed connection between the atmosphere and ocean in ENSO. However, there are a few different conceptual mechanisms for how the thermocline – the boundary between the warm water near the ocean surface and the cold water and lower depths – influences ENSO and how the oceans feeds back on the atmosphere (Suarez and Schopf, 1988; Neelin 1991; Wyrtki 1975). Still, they all agree that ENSO is a coupled phenomenon, meaning that the ocean and atmosphere are both important, with a broad spectral peak, meaning that it is only quasi-regular, repeating in this case every 2–7 years.

Suarez and Schopf (1988) suggested a (by now classical) delayed oscillator as a conceptual explanation for ENSO to naturally switch back and forth between its neutral, positive,

and negative phases. However, at least with their parameter settings, their model would only generate spectral peaks at the QB periods, and not the observed dominant peak at the 4–7-yr periods. Therefore, it can explain the biennial timescale, as while there is not a spectral peak in the QB range, the eight-month delay time is consistent with a QB extent of individual ENSO events. Note that one may be tempted to try to link biennial variability in ENSO to the stratospheric Quasi-Biennial Oscillation (QBO) (see, for example, Xie (2014), who found that stratospheric arctic ozone anomalies can lead ENSO changes by around 20 months). However, the QBO is far too regular to explain ENSO variability, which is of a much more sporadic and broadband nature, and, hence, the delayed oscillator dynamics is a far more likely candidate to explain the QB component of ENSO variability. Jajcay et al. (2018) identified a singular role of biennial variability in the causality analysis of the observed ENSO variability and the lack of such causal link in state-of-the-art climate models, despite the absence of the QB peak in the observed ENSO spectra.

To explain the observed low-frequency 4–7-yr component of ENSO, some authors have invoked a recharge mechanism repeating in a lower frequency band, driven largely by coupled interactions of SSTs with wind stress and the thermocline, taking a longer time than the QB delay mechanism, which is primarily driven by the ocean only (Wang and Ren, 2020; Bejarano and Jin, 2008). The broadness of the 4–7-yr spectral peak reflects a substantial irregularity in the ENSO event occurrence (see, for example, Jin et al., 1994), which extends to longer time scales as well. ENSO is affected by ocean currents and their associated heat transports to higher latitudes and vice versa, so various papers have searched for teleconnections to the midlatitudes and possibly polar regions to explain ENSO's irregularity and low-frequency variability. Ding et al. (2015), Furtado et al. (2012), among others, have looked at connections between ENSO and

the Pacific Decadal Oscillation (PDO), which, as its name implies, varies on a decadal timescale. Farneti (2014) built an idealized model to explain how tropical SST anomalies changed North Pacific temperature gradients and thus wind stress, which then acts to change horizontal movement and overturning of ocean water in the North Pacific. While Farneti et al. were primarily studying decadal and longer timescales, the model this team produced lead to similar results to ENSO, with quasi-regular peaks of quasi-biennial ENSO events every 4–5 years on average

In this study, we conjecture that ENSO's QB range, with periods from 18 to 42 months, is due to tropical, delayed-oscillator dynamics, as previous studies have argued. However, we hypothesize, building on Farneti et al.'s (2014) work, that ENSO's LF variability, in the range of about 4–7 years, or 42–84 months, is driven mainly by tropical-extratropical interactions. To investigate these hypotheses, we will look at composite time series of El Niño events (section 3) and maps of ENSO's total and QB-filtered variance, as well as maps of these variance ratios (section 4). Additionally, we will check how ENSO's variance and variance ratios have changes in the 18-42 and 42-84 month ranges over time, and investigate the dominant patterns which optimally highlight QB variability (section 5). To connect these results to ENSO dynamics, we will look at Farneti's idealized model to further investigate interactions between ENSO's QB and LF modes (section 6). Finally, we will assess CMIP5 global climate models to see how they handle ENSO according to some of these analyses (section 7). We will summarize our results in section 8 and outline future research directions in section 9.

2. Data and Methods

Data. This study uses monthly surface air temperature (SAT) data from the 20th Century Reanalysis V2c, interpolated onto a 2.5x2.5-degree grid, for each month from January 1880 to December 2005. We also look at the same years and same data resolution (1512 months x 73 latitudes x 144 longitudes) for 111 runs of 17 CMIP5 global climate models (GCMs) studied in Kravtsov and Callicutt (2017), Kravtsov (2017), Jajcay et al. (2018) and Kravtsov et al. (2018).

Before any analysis, the temperature at each grid point is linearly detrended and has its mean removed. Next, one can remove the seasonal cycle either by subtracting the mean temperature of each grid point at each month, or by a linear regression with the first 5 harmonics; both produce very similar results. A bandpass filter is used to isolate various bands of monthly data, most often 18-42 months, a quasibiennial (QB) range. An adaptive bandpass filter was investigated early in this study, but it was not all linear, which meant that filtering each grid point and then computing the Niño 3.4 index, or computing the Niño 3.4 index and then filtering it, yielded different results, which was problematic. A simple bandpass filter made of two low-pass FFT filters works quite well – one to remove high frequencies, and one to remove low frequencies - more effectively and efficiently, and produces the same results regardless of order of operations. The Niño 3.4 index is then derived from the average temperature anomaly in a region of the central and eastern tropical Pacific, from 5°N to 5°S, 120°W to 170°W.

Compositing. Composite El Niño time series events are formed by finding peaks of at least 1 standard deviation and at least 6 months away from any already counted peak in the Niño 3.4 index after removing its seasonal cycle, and the 84 months before and after the peak. These time series for a given ensemble member are averaged together, showing the composite El Niño

event for a given ensemble member. The composites from each ensemble member of a model or reanalysis are averaged together to show the mean composite.

Maps of variance and QB variance ratio. Temperature variance is mapped by removing the seasonal cycle from each grid point and calculating the variance in temperature anomalies at each point. QB temperature variance maps are from temperature variance after removing the seasonal cycle and filtering each grid point's temperature time series through a QB bandpass filter. Quasibiennial variance (QBVAR) maps show the quotient of QB variance and (non-seasonal) variance at each grid point.

Evolution of ENSO variance. Niño3.4 variance is also shown in time. QB Niño 3.4 and LF Niño 3.4 are calculated for each month as the Niño 3.4 index after going through a bandpass filter for 18-42 months (QB) or 42-84 months (low frequency/LF). A running window of 10, 15, or 20 years for these time series show how variance, QB variance, and LF variance change over time, calculated as the variance of a section of the time series of Niño 3.4, QB Niño 3.4, or LF Niño 3.4 in the 10, 15, or 20 years centered on that month. QB and LF variance ratios are also computed for each window, as the quotient of QB or LF variance over regular variance.

Discriminant Analysis (DA). Schneider and Held (2001) used a technique called discriminant analysis to optimally distinguish between the surface temperature's spatial patterns associated with fast and slow processes. Here we want to apply this technique to determine what spatial patterns will maximize our biennial variance ratios at any given section of the world.

To do so we first remove the mean and seasonal cycle from the data set, in this case, four different regions, 30N-30S, 60N-60S, and 30N-30S oceans only, and 60N-60S oceans only, with monthly ensemble mean 20CR data. Then, one finds the principal components and runs each component through the earlier mentioned 18-42 month bandpass filter.

From there, one can select a certain number, which we call Kstar, of PCs and filtered PCs, and make covariance matrices from each of them. A new matrix called M is the cross product of the inverse of the unfiltered covariance matrix, and the filtered covariance matrix. Once M is computed, one can find the Kstar largest eigenvectors of M in descending order of magnitude, and call this V.

The time series of our largest discriminating pattern is found my cross multiplying the PC matrix with the first column of the eigenvector matrix, and one can do this with either the unfiltered or filtered data. Finally, the first discriminating pattern is from the cross product of the inverse of our temperature data, with the mean and seasonal cycle removed, and weighed by latitude, and the quotient of the first time series divided by its standard deviation. This gives us a pattern that we can map, essentially showing us what regions will maximize the QB variance ratio for a given area.

This procedure finds the linear combinations of raw and bandpass filtered PCs that produce the time series with the highest ratio of biennial to total variance. This time series is called the canonical variate. The regression of the original spatially extended time series onto the CV is called the discriminating pattern (DP).

The CVs and DPs can be found in the subspaces of EOF defined by the first Kstar modes. If Kstar is small, you are likely to miss the important part of the biennial variability. If Kstar is too large, you would end up with the patterns of very high BVRAT that contribute nothing to the temperature variance. Physically and practically meaningful patterns should be robust in a relatively wide range of Kstar.

One can choose several values from Kstar, theoretically from 1 to as many principal components as one would have, in this case 1511, and these may give somewhat different results.

However, higher Kstar values would include incrementally more variance, but explain less of the variance ratio, and vice-versa. Since these are already sorted in descending order, we looked mostly at smaller Kstar values, but also a few higher ones, specifically: 5, 10, 15, 20, 25, 30, 50, and 100. Additionally, one can select several regions of the planet from which to from principal components. For this study, we chose to look at four different areas: 30N-30S ocean only, since ENSO is mostly associated with tropical oceans, 60N-60S ocean only, since ENSO has teleconnections with higher latitudes, and we want to see how it may be affected by them, and those same sets of latitudes but also including land, to see if land would play a major role and make sure we would not be missing something by excluding it from the analysis.

We chose to examine the first three discriminating patterns (DPs) for each region and Kstar value, to see if most of the biennial variance ratio could be described mainly by one mode, or if a second and third mode were also consistent. By looking at a wide range of regions and Kstar values, we can see if there is consistency between them for a second or third mode that alters biennial variance ratios in ENSO.

Finally, one can directly map how much each mode contributes to the QB variance ratio by mapping the squared ratio of the filtered pattern over the unfiltered pattern. For some locations, there is very little magnitude for a given DP, so taking a ratio with it in the denominator can lead to meaninglessly high QBVARs, falsely implying that this mode would lead to a QBVAR of far greater than 1. To prevent this, and only focus on where we have meaningful amounts of variability from which to calculate a variance ratio, we mask out the areas with DP magnitudes below .05. After this, any remaining points with DP variance ratios above 1 were set to 1, as they were right by the masked areas, so they were mathematical

artifacts that represented very little variability in reality. In areas that has strong DP values, the QBVAR attributed to it never exceeded 0.5, so we set the color bar maximum at that value.

3. Composite El Niño Events

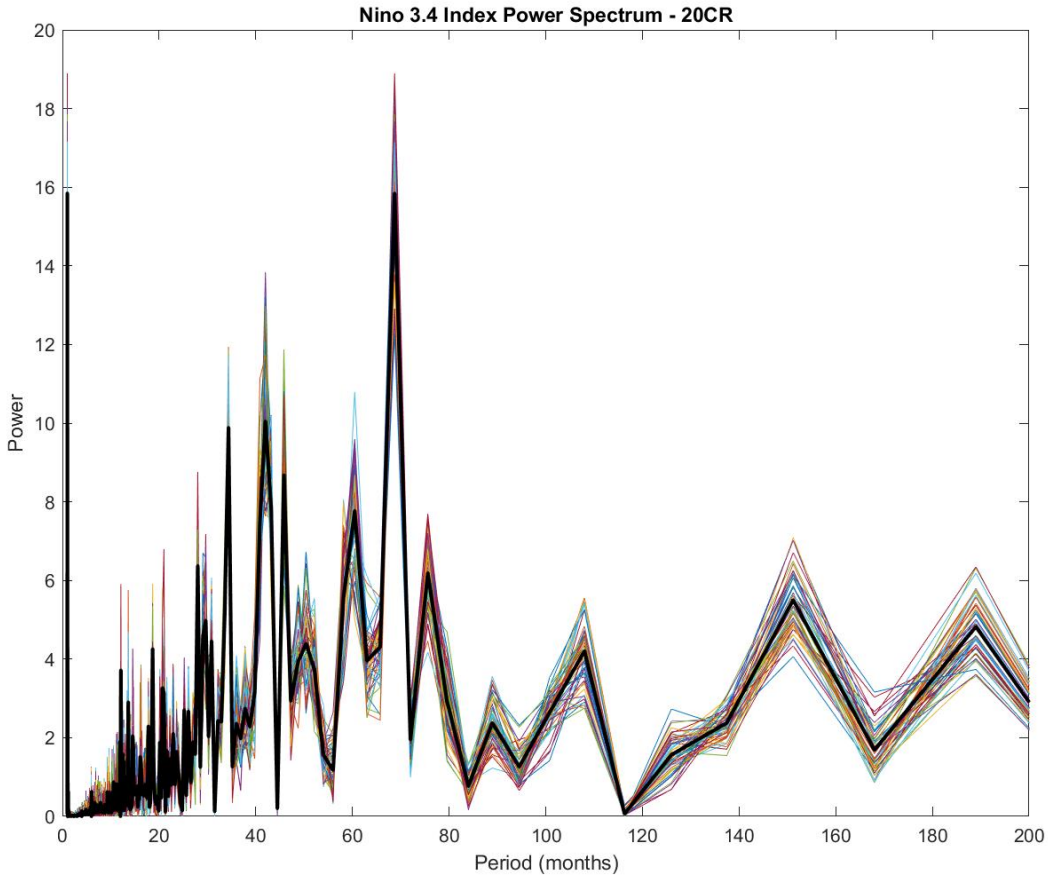

FIGURE 1: *The power spectrum for the Niño 3.4 index according to the 20th Century Reanalysis. Thin colorful lines show each ensemble member's spectrum, while the average of these 56 realizations is shown in black.*

While there is no prominent QB peak in the Niño 3.4 index's power spectrum (Fig. 1), looking at composite El Niño events can help us see variability play out in this range. We do so by finding every isolated peak in the Niño 3.4 index exceeding one standard deviation, 6 months away from any other such peak and forming composite El Niño events (averaging the ENSO time series) in the ±7-yr (84-mo) window centered on these peaks. The window half-size of 84 months was chosen as the boundary since ENSO's power drops off at lower frequencies than that. Also, to prevent a few particularly strong El Niño events from weighing more than the rest, we normalized each event by its maximum amplitude, leading to the maximum amplitude of 1 in the ENSO composites so obtained. Figure 2 shows the composite El Niño event of the Niño 3.4 index from 1880-2005 according to the 20th Century Reanalysis.

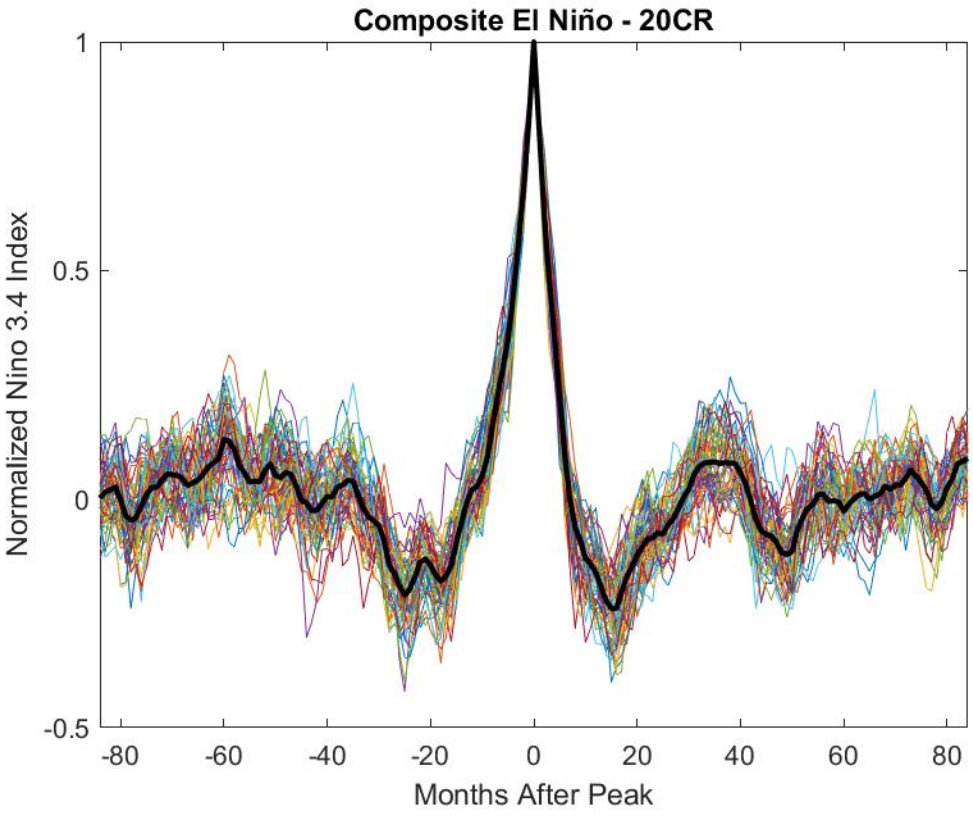

FIGURE 2: *Composite El Nino events from the 20th Century Reanalysis, for the average behavior of the Niño 3.4 index within 84 months of an El Niño peak.*

This is done for each of 56 ensemble members in the reanalysis (thin colored curves), with the average composite event shown by a black heavy curve. While the latter curve shows the mean, the individual curves give an idea of uncertainty in the 20CR data set. For all 56 ensemble members, the figure shows the typical time lag between main peaks (or troughs) of about 35–40 month, on the upper end of the QB range; this is how the composite of the damped biennial oscillator would look like (section 6). This figure therefore demonstrates significant QB variability for this ENSO index, and is one of our primary motivations for studying biennial variability, despite it not being the spectral peak for ENSO (see also Jajcay et al. 2018).

Additionally, this shows that ENSO will tends to be negative (attain a La Niña phase) about 15–20 months before and after an El Niño peak, and while it may not necessarily be enough to be a La Niña event each time necessarily, a negative ENSO value in a year before an El Niño peak is still a very common occurrence among the ensemble. Most models qualitatively reproduce the composite ENSO event, as further discussed in section 7.

ppendix shows composites for each run of 17 CMIP5 models, for 111 simulations in total. Since several of them do not have the best handle on biennial variability, or how they handle transitions to or from El Niño states in general, then improving our understanding of these timescales should help us not only in understanding ENSO better but also global climate variability in general.

4. Quasi-biennial Variance Ratios

Since we see hints of QB variability in these composite El Niño events, as shown by each ensemble member at around 36 months after a composite El Niño peak being higher than they were at 18 months after a peak, we expect that a map of variance in the data bandpass filtered

(BPF) in the biennial range should mainly highlight the eastern and central tropical Pacific, which is our main area of focus for ENSO, as well as some other areas with strong teleconnections to ENSO. The global BPF variance map (Fig. 3) highlights the tropical Pacific somewhat, but it also highlights high latitude land masses. This could make one suspect that they are strongly connected to ENSO, or at least some sort of biennial phenomenon; however, a map of variance in unfiltered temperature anomalies reveals that high latitude land simply has high variance in general, regardless of frequency (Figs. 3, 4).

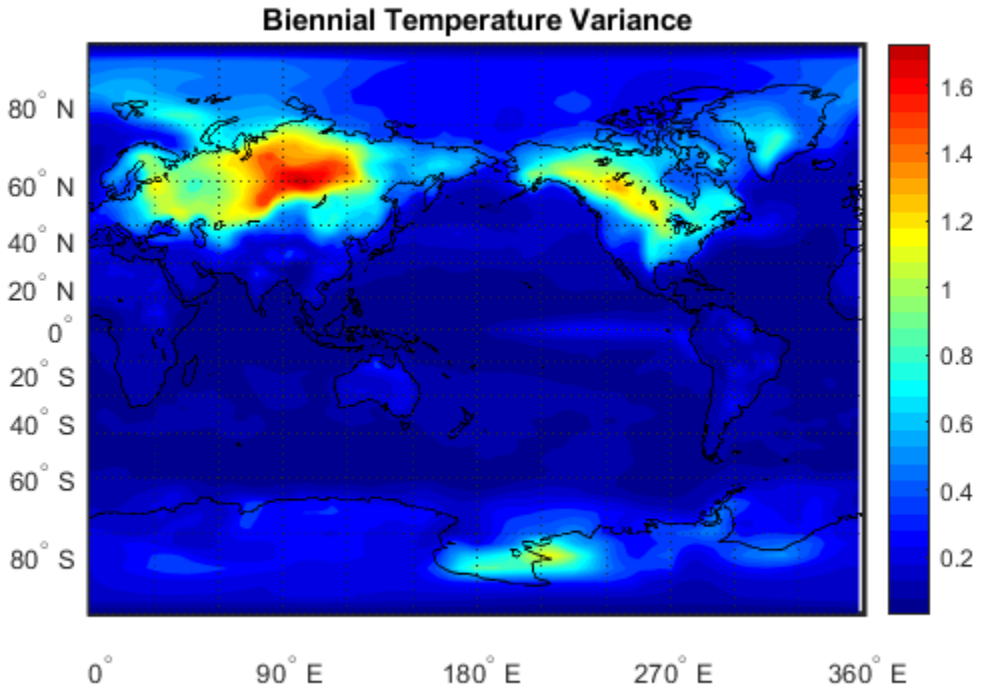

FIGURE 3: *Variance in monthly temperature anomalies after applying a biennial bandpass filter at each point on earth, according to the 20th Century Reanalysis, 1880-2005.*

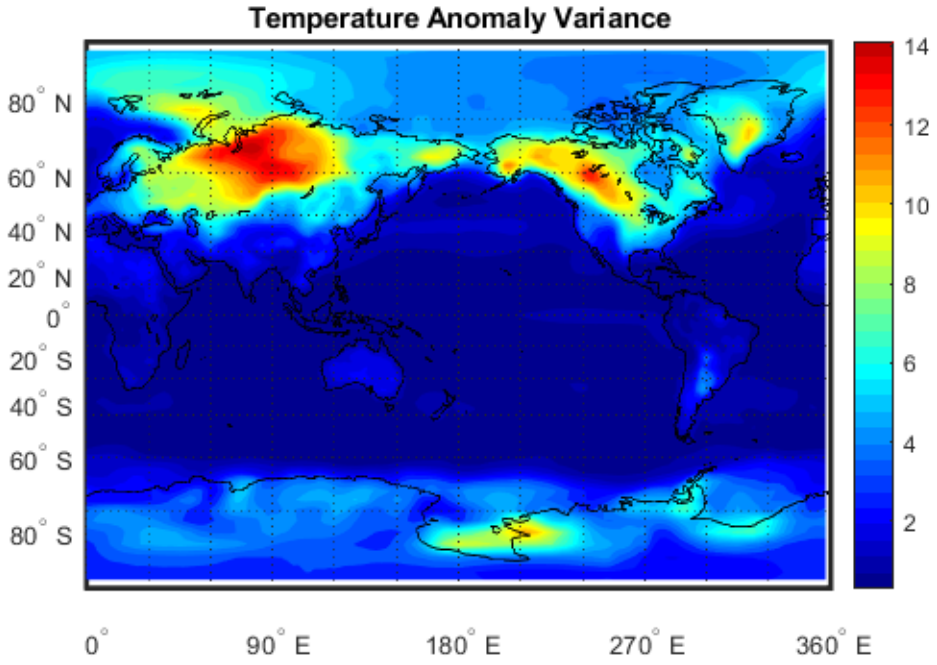

FIGURE 4: *Variance in monthly temperature anomalies after removing the seasonal cycle, according to the 20th Century Reanalysis, 1880-2005.*

Thus, we introduce a new metric, the biennial variance ratio (BVRAT). The BVRAT is simply the variance of the SST time series in the 18-42 month range divided by the variance at all frequencies after subtracting out the seasonal cycle, at each grid point. While BPF variance maps only hint at the tropical Pacific being strong in this band, and overall variance being highest in high latitude land, the BVRAT map highlights the tropical Pacific as the most important area for biennial variability, suggesting that cycles between 18-42 months are responsible for around 30 percent of all variability in temperature anomalies in the tropical Pacific (Fig. 5). In fact, tropical oceans in general have a higher BVRAT, decreasing as one goes poleward or onto land. The midlatitude Pacific has more BVRAT than that of other oceans - consistent with ENSO teleconnections being at work there (Deser et al., 2017; Ding et al., 2015)

- though it is less than that of the tropics, indicating that more of the variability there is from either higher frequency weather noise and the polar jet, or also lower frequency processes like ocean dynamics, which we will discuss later.

Like the biennial map, we have the most variance over high-latitude land, and not as much in tropical oceans. Therefore, to see if ENSO has much biennial variability, one could see what proportion of the total variance is caused by this 18–42 month range, and plot variance ratios.

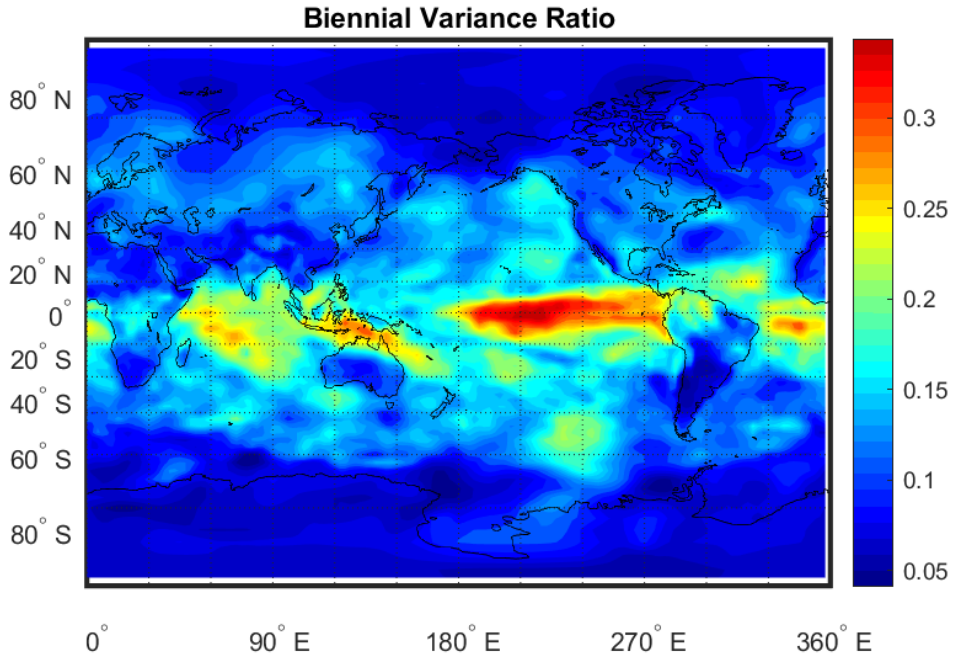

FIGURE 5: *QB variance ratios for the 20th Century Reanalysis. These are calculated as the QB variance from Figure 3 divided by the total variance from Figure 4.*

Our variance ratio analysis highlights the ENSO region, namely the equatorial Pacific, especially the central and eastern parts, as exhibiting the highest QB variance ratio. Although the

strongest areas are in the tropical Pacific, we also see locally high amounts near Australia and Indonesia, for the west side of the Walker circulation associated with ENSO, and in the tropical Indian and Atlantic Oceans as well, though less strongly than in the Pacific. One can also notice somewhat higher QBVARs in the far north Pacific than far north Atlantic, though it is weak. Finally, we see higher QBVARs over the ocean than land, as the ocean takes much longer to heat or cool thanks to water's high specific heat capacity and the ocean's depth.

High quasi-biennial variance ratios are limited to the tropics according to these figures. However, this does not necessarily mean that other areas are not affected by this variability, nor that extratropical areas cannot affect the tropics on this timescale.

This makes sense in light of earlier findings, as ENSO also has high spectral power in the 4-7 year range, and perhaps some multidecadal variability, both likely linked to ocean currents and the PDO. Although multidecadal variability is not the focus of this paper, one can see different decades of ENSO be dominated by different frequency bands, perhaps indicating different processes being stronger in different decades (Fig. 6). This figure uses another way of visualizing our biennial variance ratios. In a running window of say 10 years, or any window you choose, we can find the variance ratio within that time period. We could also do this for other frequency bands if we want to see modes that vary in other times. Additionally, while there is some debate about ENSO shifting between different modes, finding a time series of BVRATs could help with this, as well as finding some ENSO events in times of low BVRATs to explain other causes for ENSO.

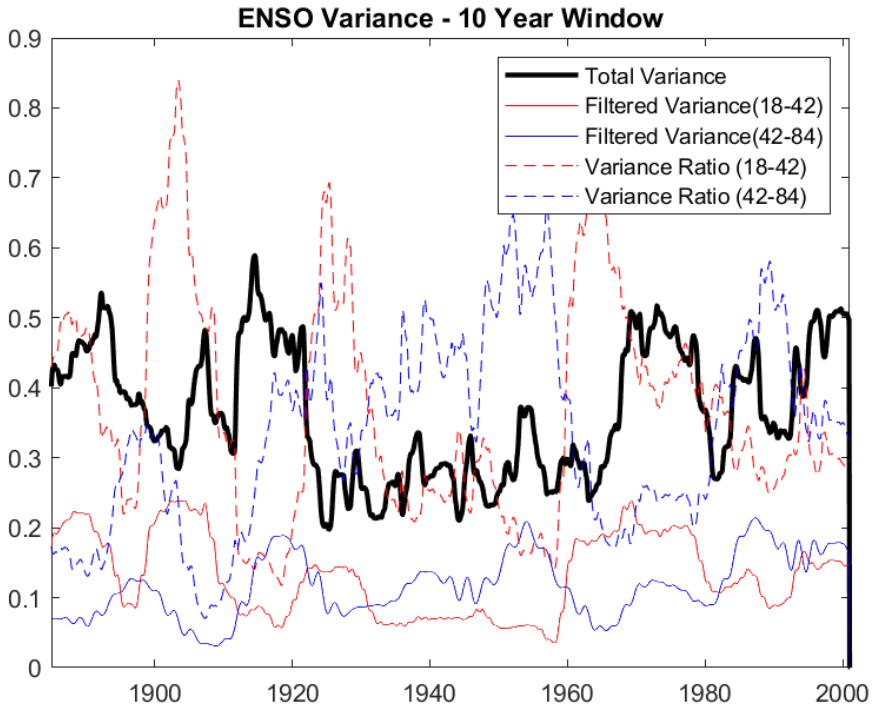
ENSO Variance - 10 Year Window
Total Variance
Filtered Variance(18-42)
Filtered Variance(42-84)
Variance Ratio (18-42)
Variance Ratio (42-84)
0.9
0.8
0.7
0.6
0.5
0.4
0.3
0.2
0.1
0
1900
1920
1940
1960
1980
2000

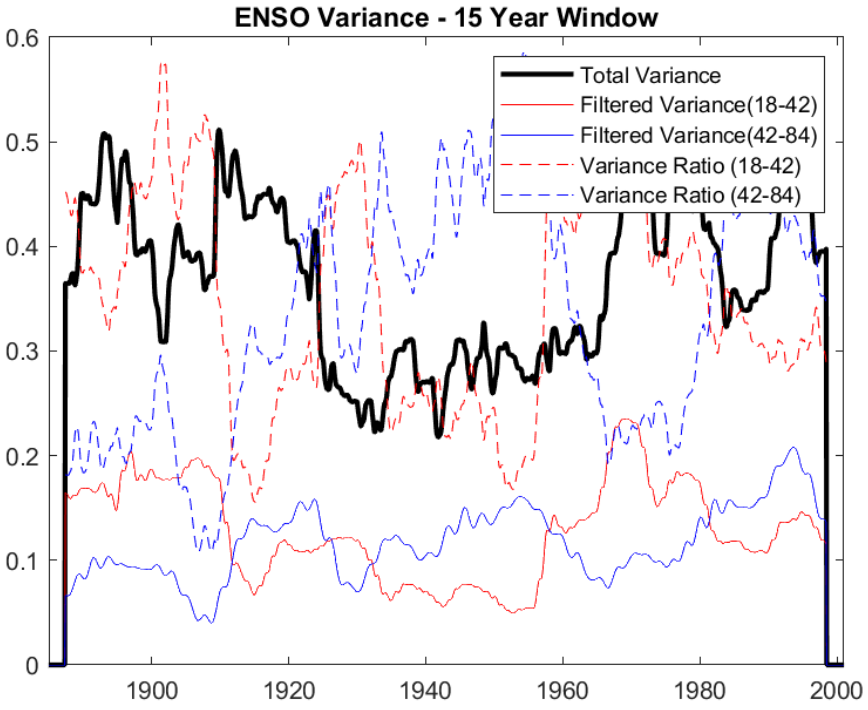
ENSO Variance - 15 Year Window
Total Variance
Filtered Variance(18-42)
Filtered Variance(42-84)
Variance Ratio (18-42)
Variance Ratio (42-84)
0.6
0.5
0.4
0.3
0.2
0.1
0
1900
1920
1940
1960
1980
2000

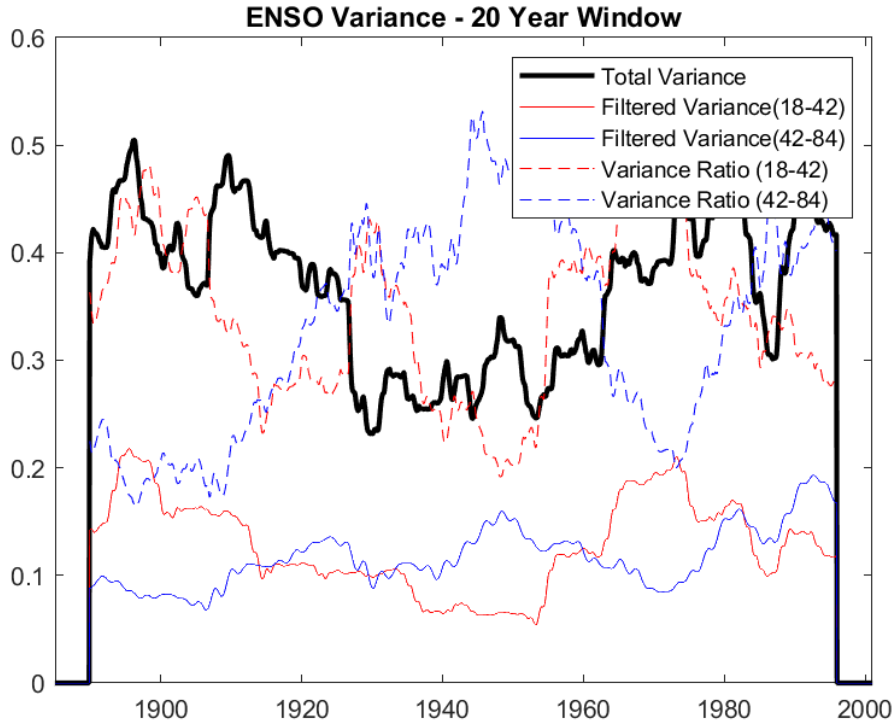

***FIGURE 6**: Time series of variability and variance ratios for the 18-42 month QB band, as well as the 42-84 month LF band, calculated from 10, 15, and 20 year running windows centered at each month of the Niño 3.4 index according to monthly data from the 20th Century Reanalysis after removing the seasonal cycle.*

By centering a 10-year window at each month in our time series, we can see not just ENSO variability, but also QB variability and even the QBVARs change with time. Of course, in decades with a lower variance ratio for a certain frequency band, this would suggest that any variability would need to come from some other frequency band. So, one could also view the 18-42 month band vs the 42-84 month band, the lower-frequency side of the often written 2-7 year peak for ENSO. Figure 6 shows that in some decades, 18-42 month frequencies do more, while in others, 42-84 month cycles do more for ENSO. This also lines up fairly well with findings from Wang and Ren (2020) that ENSO is sometimes driven more by an approximately 3 year mode, and sometimes driven more by an approximately 5 year mode, which can lead not only to temporal but also spatial diversity in ENSO.

Wang and Ren cite Bejarano and Jin (2008), who found that the QB mode of ENSO is likely from from a reflective-advective oscillator; this lines up with Suarez and Schopf's (1988) that QB behavior in ENSO is from a delayed oscillation of reflected equatorial waves with a period around 2-3 years. Bejarano and Jin (2008) also found that 4-7 year variability is connected to a decrease in equatorial wind and buildup of heat across the Pacific basin. These timescales are different because the 4-7 year mode depends on wind stress anomalies in the Pacific, while the QB mode is more ocean-driven (Wang and Ren, 2020). Wang and Ren (2020) and Bejarano and Jin (2008) both find that these QB and LF modes are influenced by multidecadal variability, and Figure 6 is in line with these findings.

This analysis would suggest that multidecadal variability could influence the processes that cause these different mechanisms, and that better understanding of multidecadal processes could help models have more accurate QB and LF variability. In observations, QB and LF variance changes on different decades, suggesting decadal variability influences these two modes.

We will return to the theme of connecting QB and LF processes to decadal variability in section 6. First however, we want to confirm that QB variability, while having its highest variance ratio in the tropics, is indeed caused mainly by tropical processes. To do so, we next perform discriminant analysis of surface temperature records designed to highlight the spatially extended modes of quasi-biennial variability.

5. Discriminating Patterns of QB Variance Ratios

Figure 7 shows DPs and their QBVARs computed for surface temperatures over tropical oceans only. Regardless of Kstar, the first DP shows high magnitude in the central and especially

eastern tropical Pacific, strongly resembling a typical ENSO temperature anomaly. Additionally, each pattern looks similar in shape between the unfiltered and filtered patterns and is usually weaker in magnitude for the filtered data.

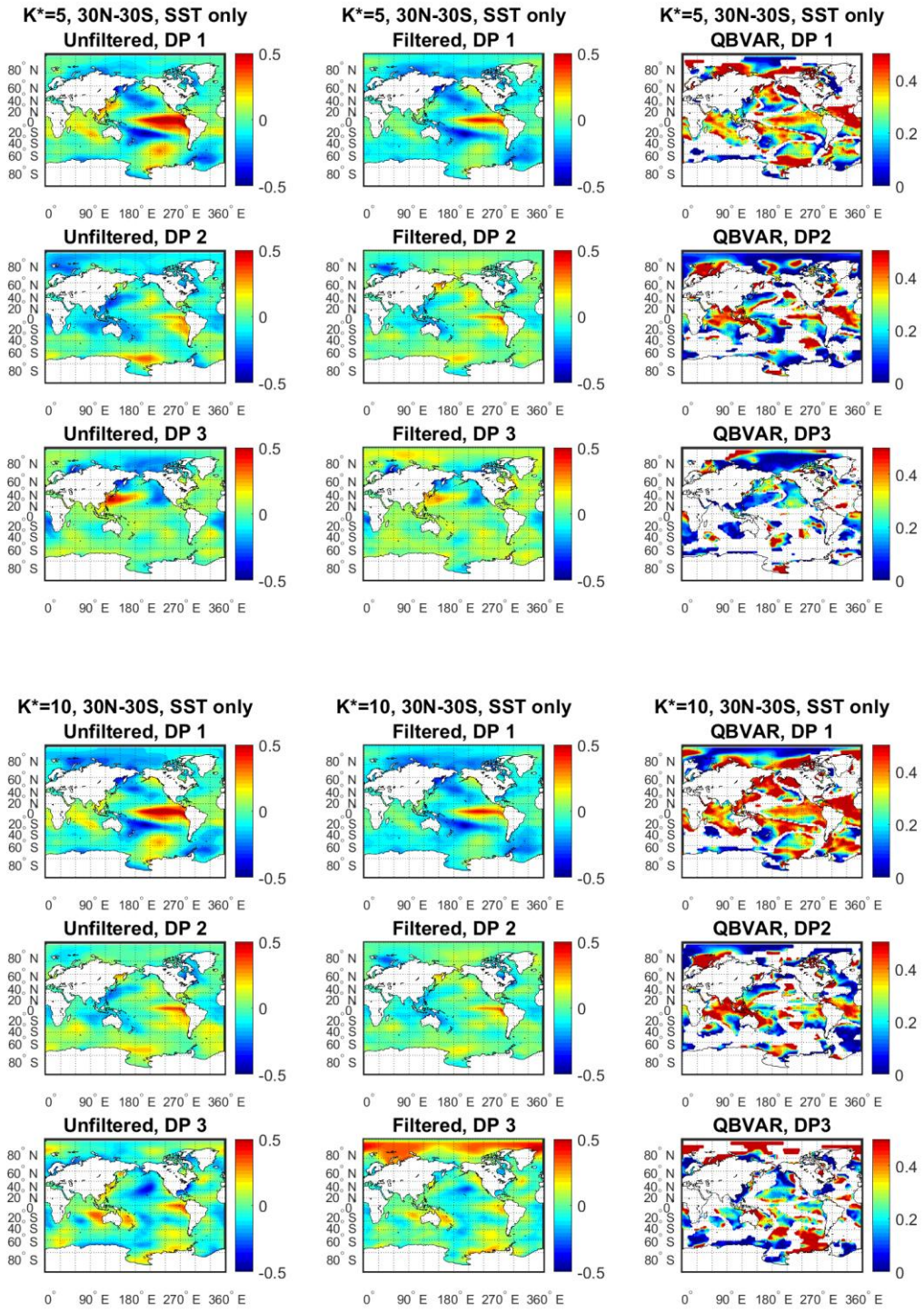

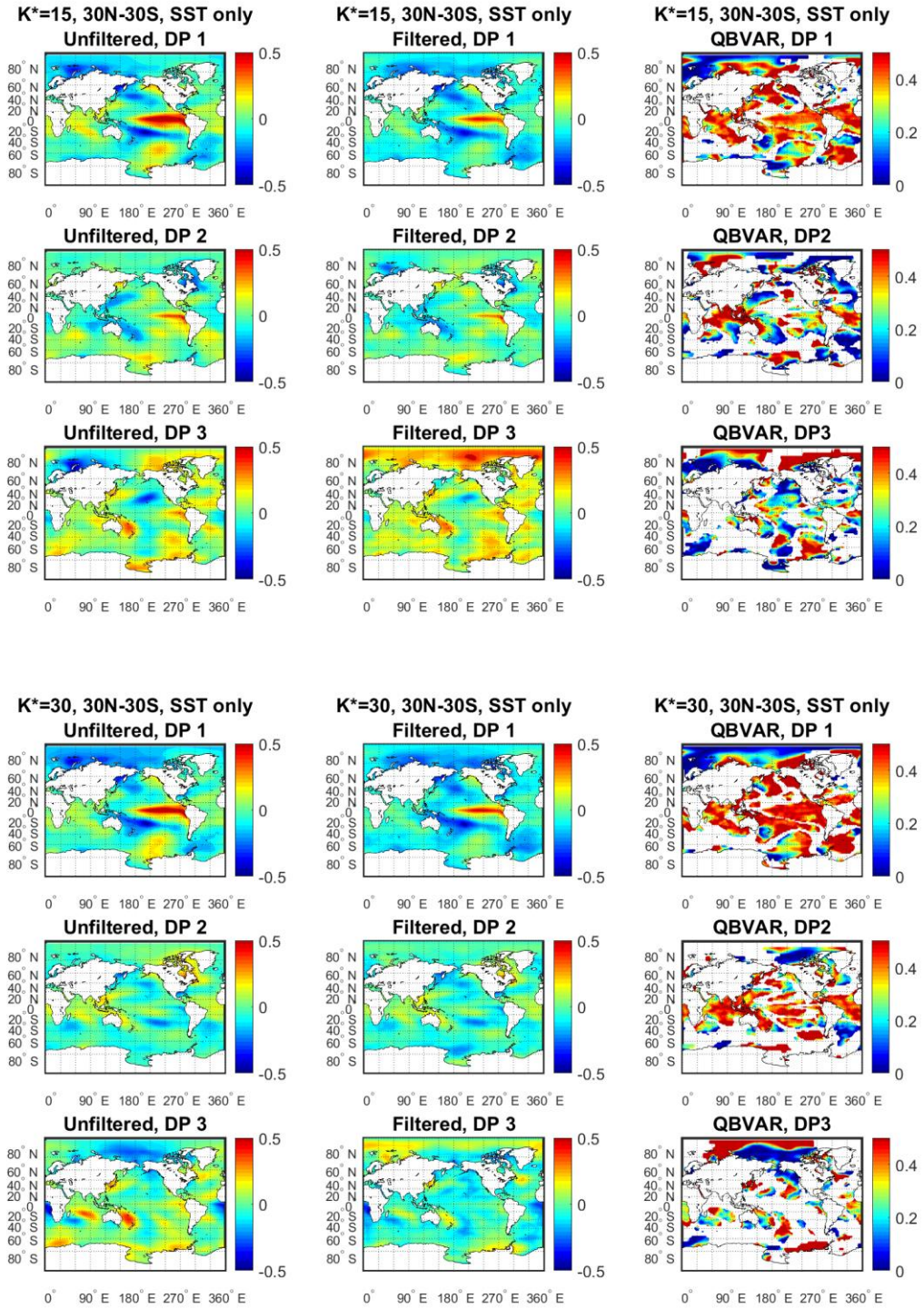

FIGURE 7: *The first three discriminating patterns and associated QBVARs for SSTs from 30N to 30S.*

At least in the maps computed from tropical waters only, we find only one consistently strong mode, as the second DP is far weaker than the first, and the third DP hardly as any spots in the Pacific with a significant variance ratio. The third mode seems to resemble the PNA, as its strongest spots are near the west coast of North American and the east coast of Asia, staying confined to the midlatitudes. A weak second mode appears somewhat consistently, though its spatial pattern changes somewhat from map to map depending on K^*. This was also true with other Kstar values we checked. However, we should also look at other regions before ruling out the possibility of a strong second mode in the QB range.

Figure 8 shows the DPs calculated from surface temperature over the oceans from 60N to 60S, thus potentially including influence from higher latitudes. If a mode does not express strongly in the tropics, this would indicate that it primarily affects higher latitudes only.

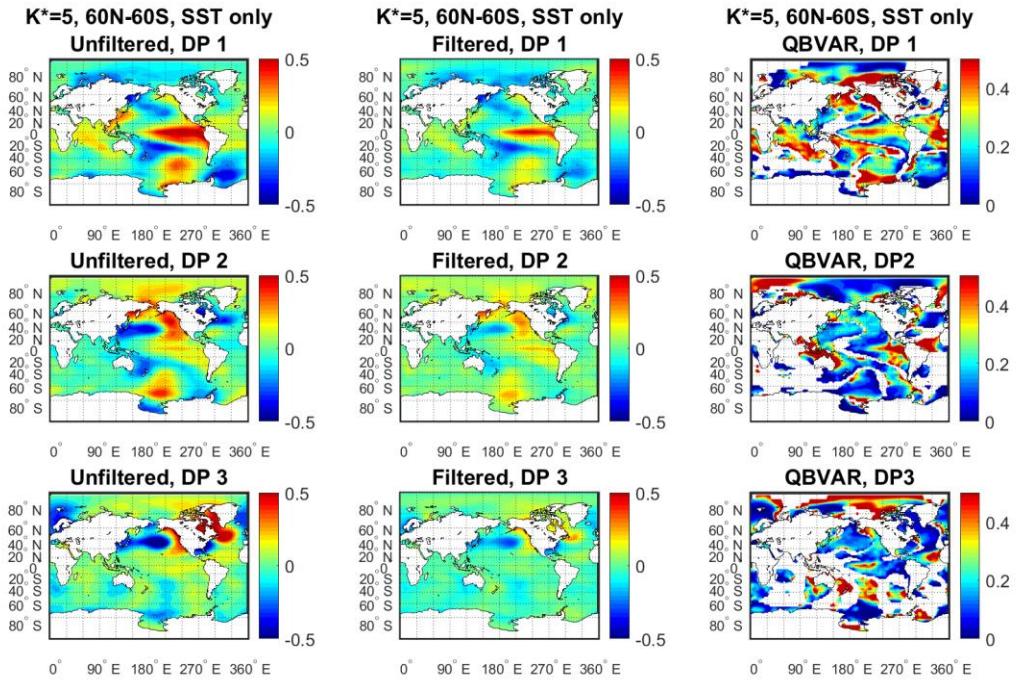

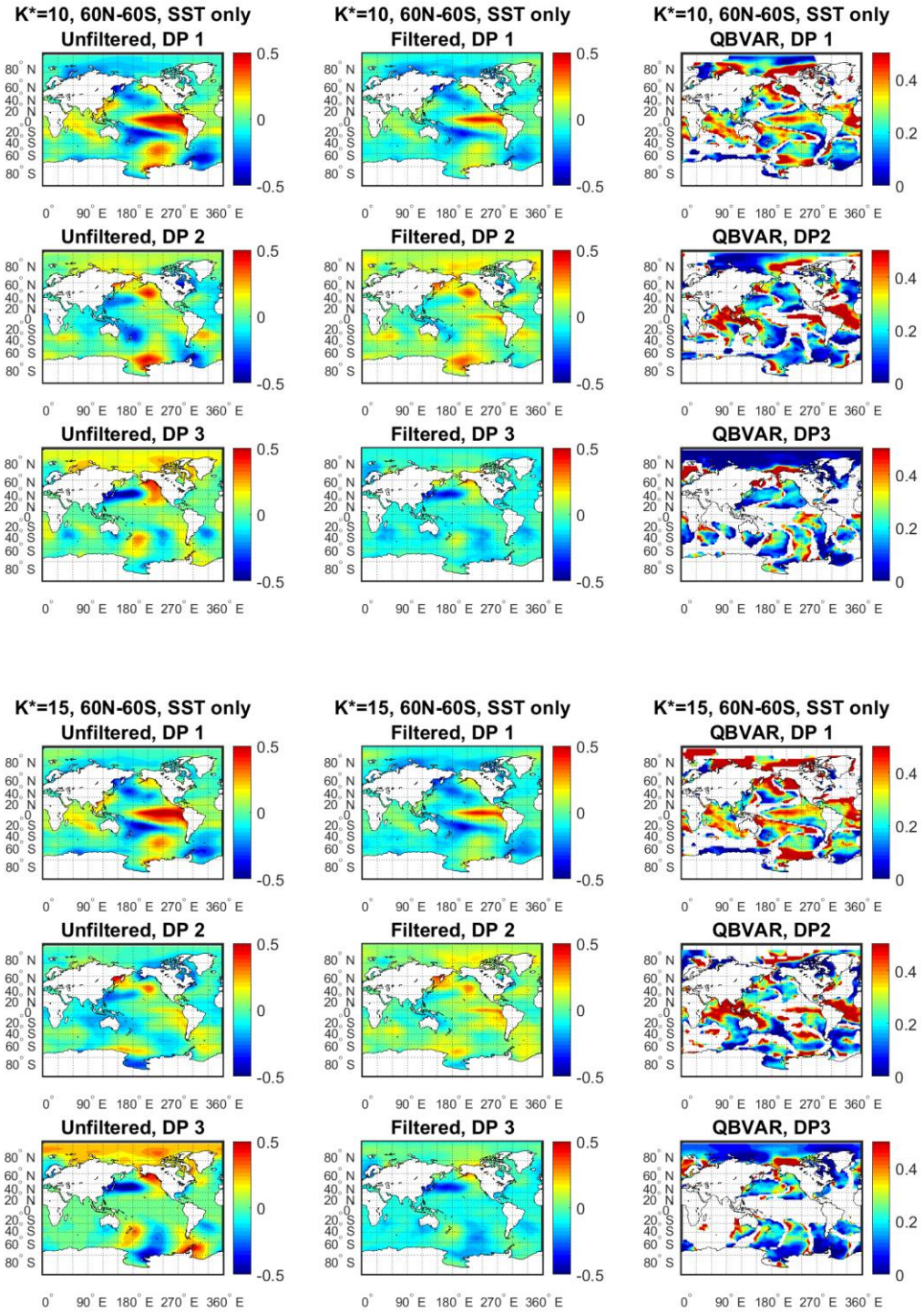
K*=10, 60N-60S, SST only
Unfiltered, DP 1
Filtered, DP 1
QBVAR, DP 1
Unfiltered, DP 2
Filtered, DP 2
QBVAR, DP2
Unfiltered, DP 3
Filtered, DP 3
QBVAR, DP3
K*=15, 60N-60S, SST only
Unfiltered, DP 1
Filtered, DP 1
QBVAR, DP 1
Unfiltered, DP 2
Filtered, DP 2
QBVAR, DP2
Unfiltered, DP 3
Filtered, DP 3
QBVAR, DP3
80° N 60° N 40° N 20° N 0 20° S 40° S 60° S 80° S
0° 90° E 180° E 270° E 360° E
0.5 0 -0.5
0.4 0.2 0

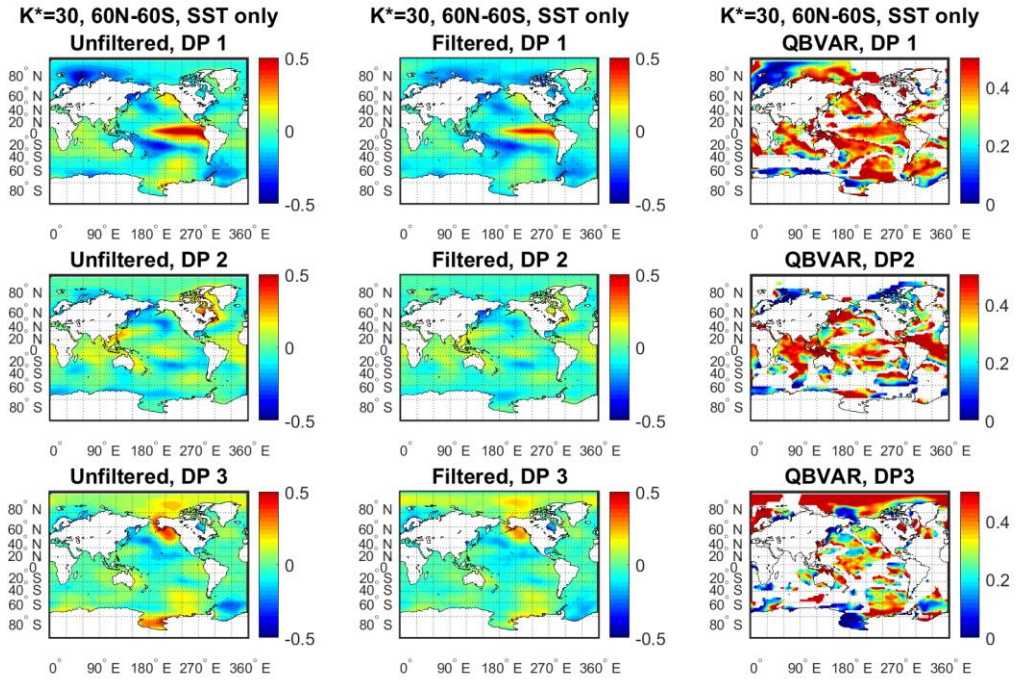

FIGURE 8: *The first three discriminating patterns and associated QBVARs for SSTs from 60N to 60S.*

In each of these, our leading pattern is still strongest in the central and eastern equatorial Pacific, with a high QBVAR across most of the Pacific. A second pattern appears to be strong in the North Pacific, showing opposite signs in the waters near Asia vs North America, though this fades at higher Kstar values, and does not have a strong QBVAR in most of the tropical Pacific, indicating that while it may be a strong mode for the midlatitudes, it does not have a strong effect on ENSO in QB frequencies. However, at higher Kstar, we do see a higher QBVAR from the second mode in the central tropical Pacific, perhaps indicating that while it is not very strong on this timescale, it does not rule out the possibility that it may be stronger on a different timescale, such as the LF scale of 4-7 years.

So far, these DPs indicate that most of ENSO's variability on the QB timescale is from tropical mechanisms only, with much less influence from higher latitudes, though they cannot be

discounted entirely on this timescale. Still, one should check DPs that include land in the calculation as well, for a more thorough result. The next figures show DPs from the full surface between 30N-30S, and then between 60N-60S (Fig. 9).

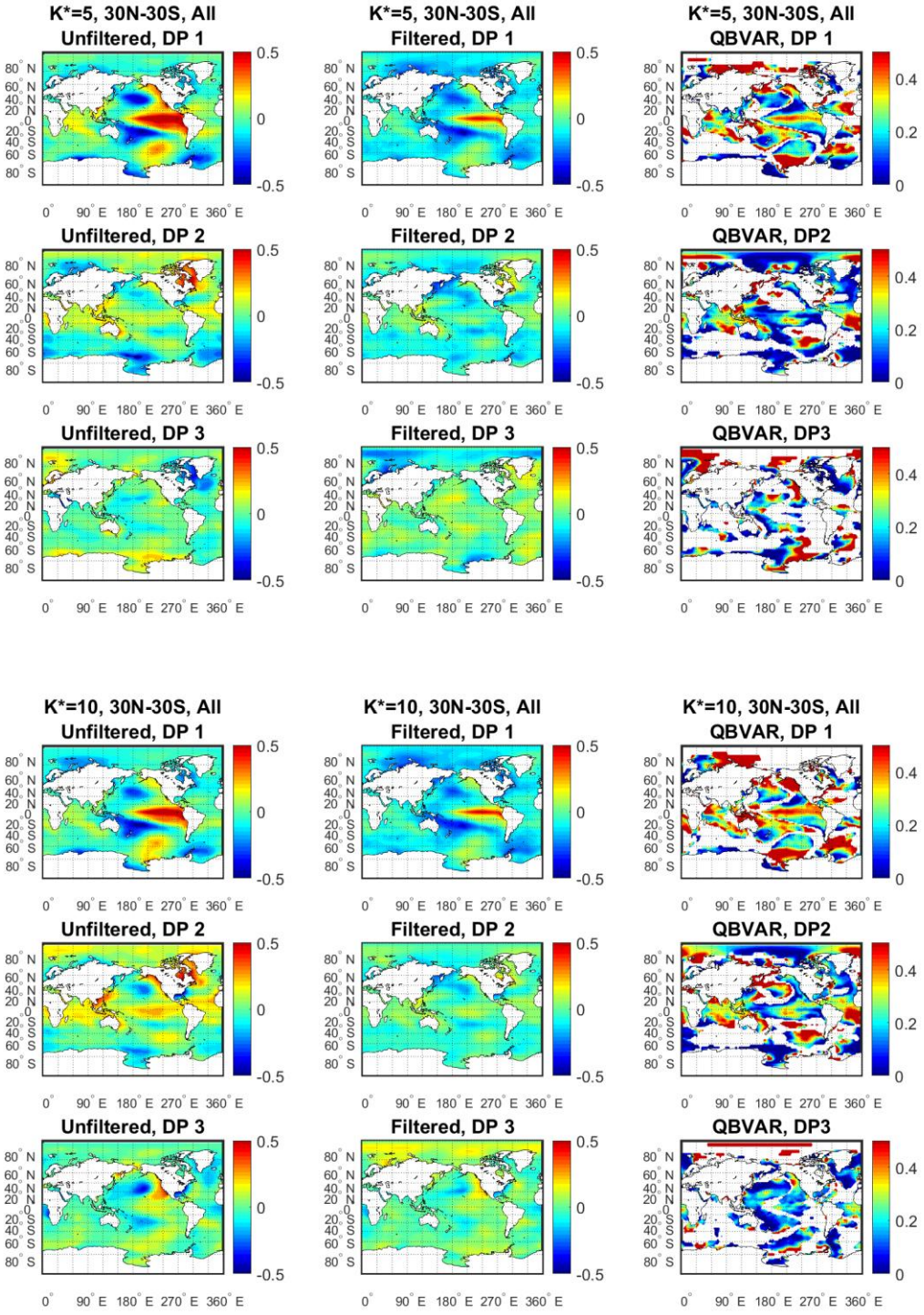

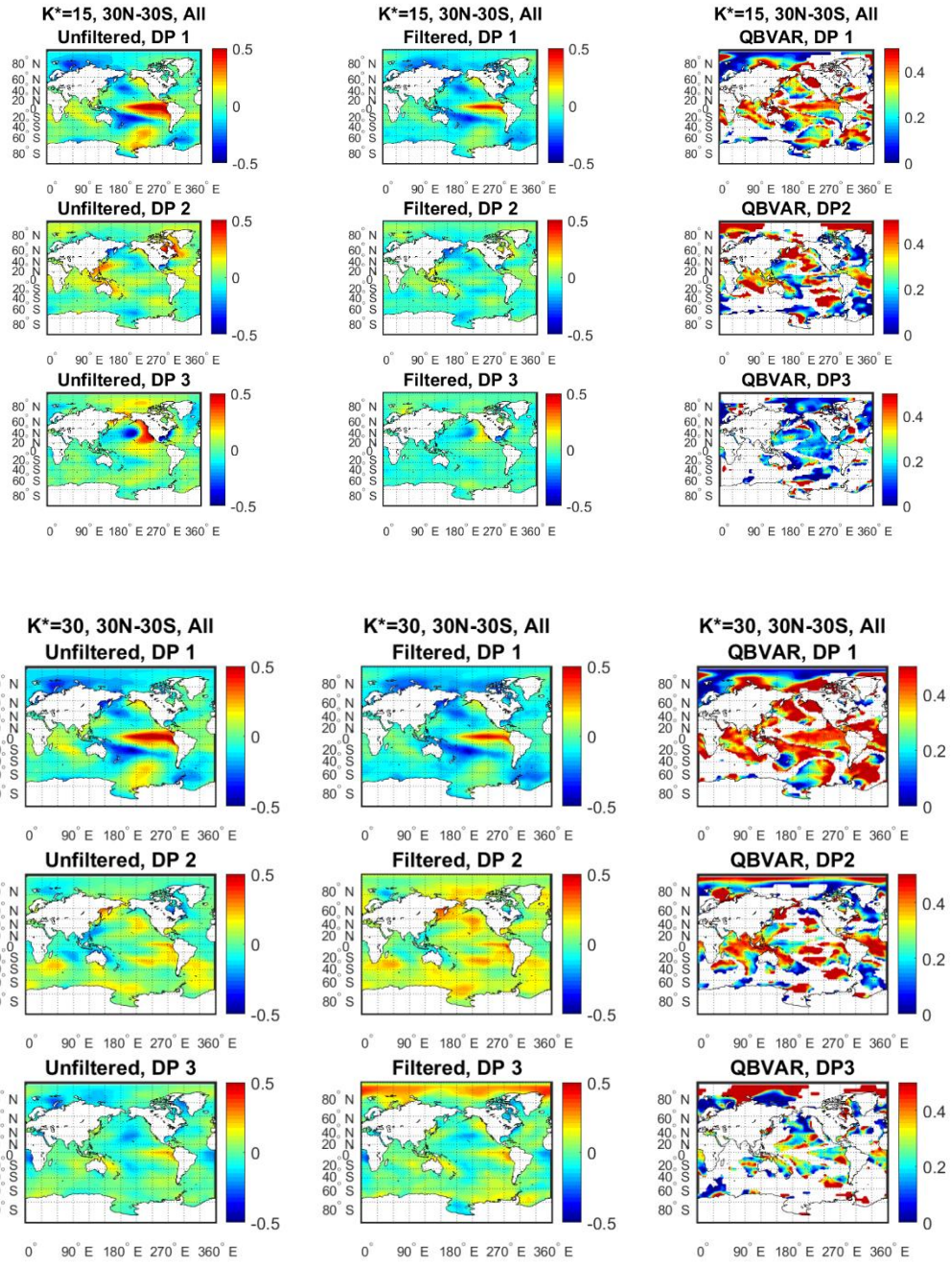
K*=15, 30N-30S, All
Unfiltered, DP 1
Filtered, DP 1
QBVAR, DP 1
Unfiltered, DP 2
Filtered, DP 2
QBVAR, DP2
Unfiltered, DP 3
Filtered, DP 3
QBVAR, DP3
K*=30, 30N-30S, All
Unfiltered, DP 1
Filtered, DP 1
QBVAR, DP 1
Unfiltered, DP 2
Filtered, DP 2
QBVAR, DP2
Unfiltered, DP 3
Filtered, DP 3
QBVAR, DP3
80° N 60° N 40° N 20° N 0 20° S 40° S 60° S 80° S
0° 90° E 180° E 270° E 360° E
0.5 0 -0.5
0.4 0.2 0

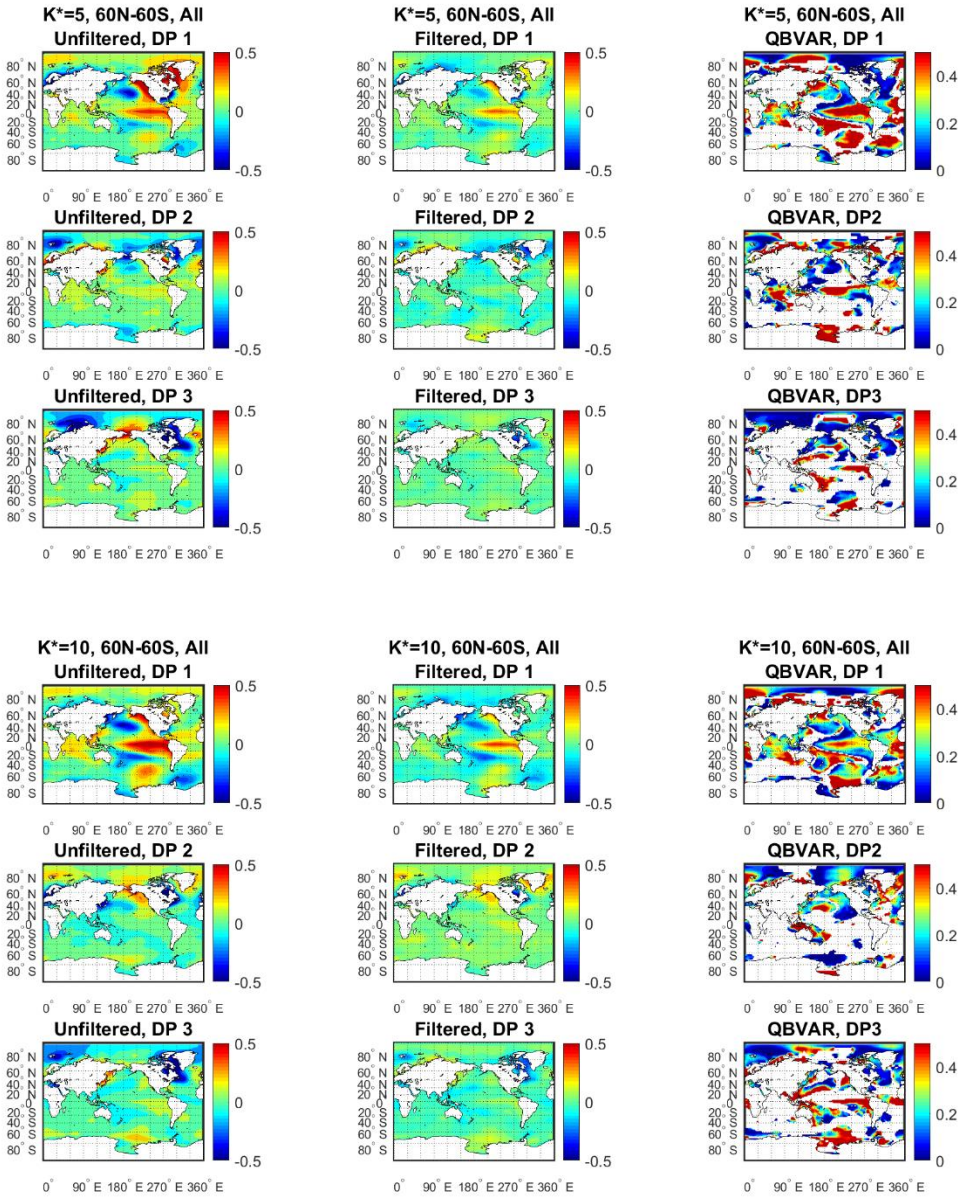
K*=5, 60N-60S, All
Unfiltered, DP 1
Filtered, DP 1
QBVAR, DP 1
Unfiltered, DP 2
Filtered, DP 2
QBVAR, DP2
Unfiltered, DP 3
Filtered, DP 3
QBVAR, DP3
K*=10, 60N-60S, All
Unfiltered, DP 1
Filtered, DP 1
QBVAR, DP 1
Unfiltered, DP 2
Filtered, DP 2
QBVAR, DP2
Unfiltered, DP 3
Filtered, DP 3
QBVAR, DP3
0° 90° E 180° E 270° E 360° E

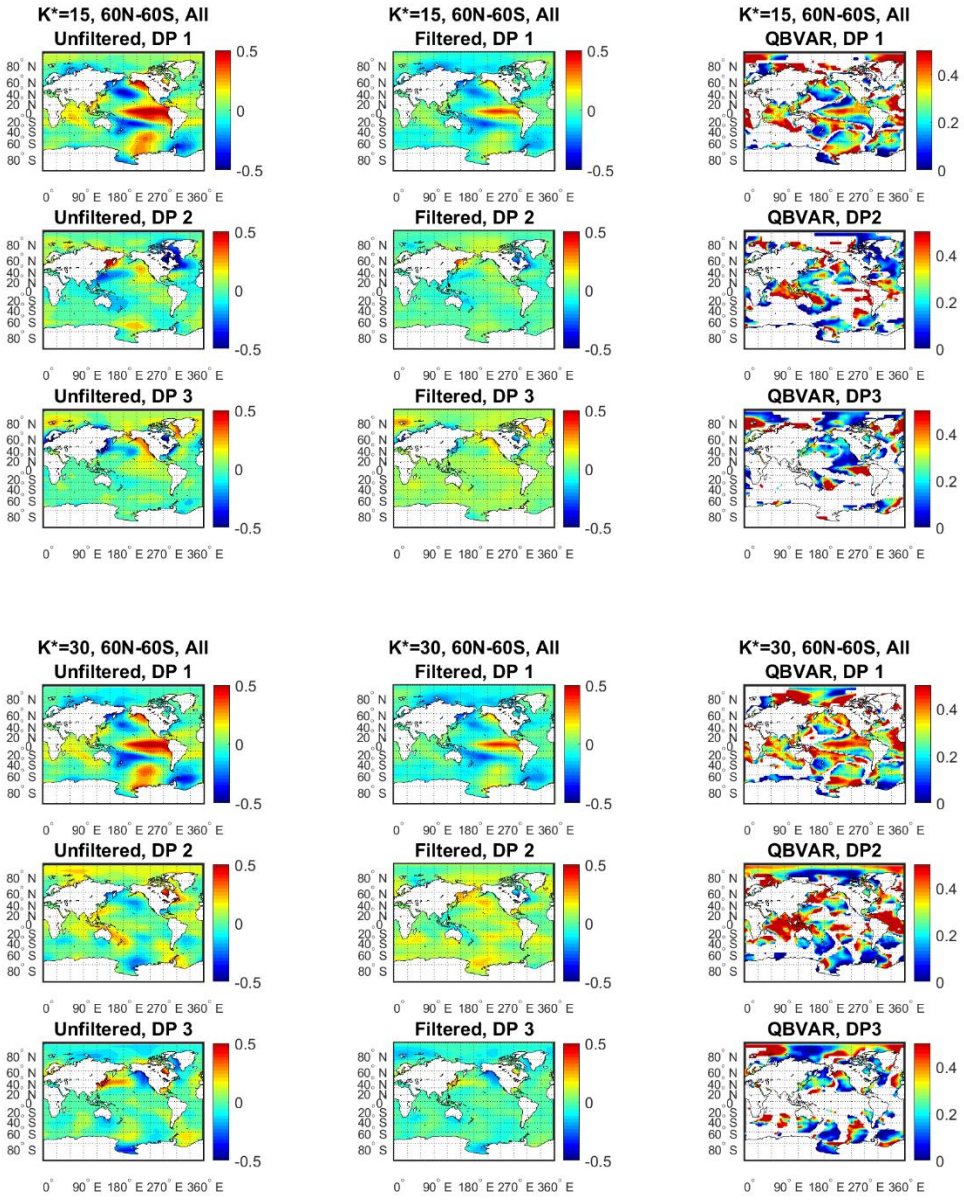

FIGURE 9: *The first three discriminating patterns and associated QBVARs for all available surface temperature data from 30N to 30S and 60N to 60S.*

As Figure 5 showed earlier, land usually has a much lower QBVAR than ocean, largely due to land heating and cooling much more quickly. Due to this, the figures that include land are not especially different from their ocean-only counterparts. There is, once again, only one mode that consistently explains most of the tropical Pacific's variability in the QB timescale. While the

second mode has only weak expression in the tropical Pacific depending on what region we choose and Kstar, it is usually stronger in the midlatitudes than the tropics, indicating that it may be weaker on this QB timescale than another, such as the LF timescale potentially, and associated more with higher latitudes.

Therefore, we can conclude that most of ENSO's QB variability and variance ratio can be attributed mainly to tropical dynamics, and that other parts of the world have less influence on this timescale. We investigated biennial variability in the first place because of the typical length of El Niño/La Niña events being closer to this timescale than the LF one, as well as our composite El Niños. However, some decades have stronger variability than others, and stronger events than others, and more of ENSO's variability is in the LF range than in the QB range, so finding a potential source for the LF and longer variability would be quite worthwhile. The inconsistent second mode that some of the DP figures alluded to on the QB timescale suggest a connection with higher latitudes influencing ENSO. In earlier figures (Fig. 6), we found that QB and LF frequencies influence ENSO more in different decades as well, so we should now discuss interannual and decadal ENSO variability.

6. Interannual-to-Decadal Variability, and Tropical-Extratropical Connections

Farneti (2014) investigated decadal variability in the Pacific, specifically by looking at interactions between tropical SST anomalies, the subtropical ocean gyre, and the subtropical (oceanic) cell. The latter two terms refer to horizontal movement of water from ocean currents, and vertical overturning of water, in the North Pacific, between the tropics and midlatitudes.

While there is already a name for decadal oscillations in the Pacific, not just in the tropics but across the whole ocean basin, the Pacific Decadal Oscillation (PDO), ENSO is generally

thought to be related to this, and Farneti et al. specifically discussed ENSO. In their idealized model for temperatures, gyre strength, and cell strength, they found and discussed decadal and multidecadal variability that lined up with observations quite well. However, one result of his that he did not discuss much was that this model also produced strong 4-5 year variability, lining up quite well with ENSO, though also stronger QB variability than the data shows, due to being based on an oscillator with a QB period. Figure 10 shows the result of Farneti's model, showing a maximum usually every 4-7 years for SSTs in the central tropical Pacific.

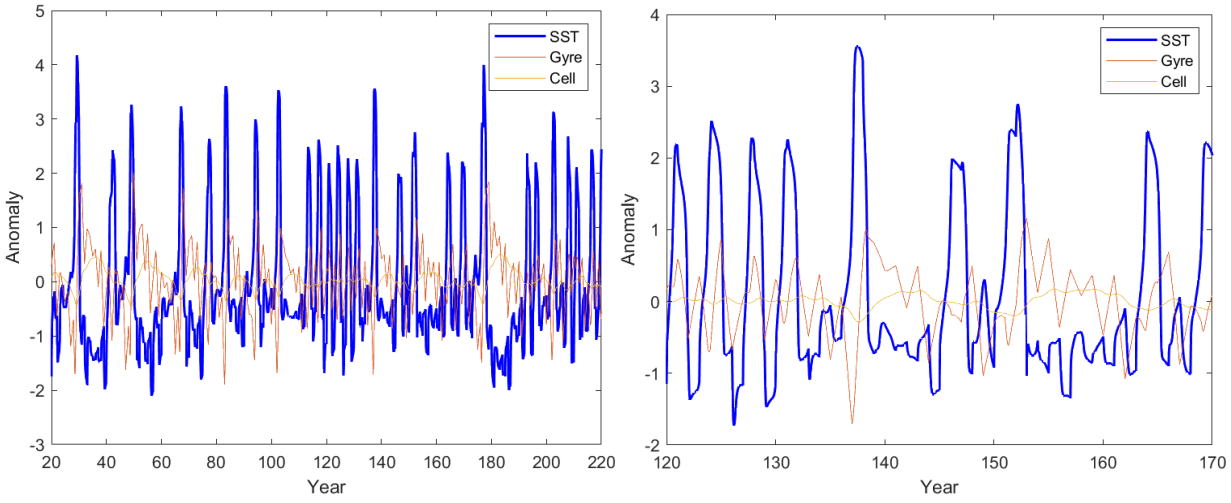

FIGURE 10: *SST, subtropical gyre intensity, and subtropical cell anomalies from Farneti's model, analogous to Figure 14 in Farneti (2014). Years are counted from initialization, with 200 years shown (left), and 50 years shown for detail (right).*

Farneti et al. (2014) investigated how tropical SST anomalies would affect subtropical wind stress, and in turn, alter ocean currents and heat transport in the Pacific, mainly the North Pacific. The team found a connection between tropical SST anomalies and wind stress in the North Pacific on decadal timescales.

Section 4 of Farneti et al. (2014) put forth an idealized model to discuss their proposed feedbacks between tropical Pacific SSTs associated with ENSO, the subtropical gyre, and the subtropical cell. The model is based on the delayed oscillator by Suarez and Schopf (1988),

though it adds a term to the temperature equation: EG, where G is the strength of the idealized subtropical gyre, and E is an exchange coefficient. The model is a system of three ordinary differential equations, with values for constants derived from earlier parts of Farneti's study.

Suarez and Schopf's original 1988 delayed oscillator for ENSO is of the form:

$$\frac{dT}{dt} = T - \alpha T(t-\delta) - T^3 \quad (1)$$

Farneti altered this SST equation to:

$$\frac{dT}{dt} = T - \alpha T(t-\delta) - r1(T-T0)^3 - EG \quad (2)$$

In equation (2), T0 represents an equilibrium temperature proportional to the upwelling anomaly from the subtropical cell:

$$T0 = -\beta C \quad (3)$$

In (3), C is the term for the subtropical cell strength, while β is set to 2 for equilibrium.

C, the idealized strength of vertical motion of water in the subtropical cell is given by:

$$\frac{dC}{dt} = -K(C-G) \quad (4)$$

Equation (4) means that a spin up of the subtropical gyre will lead to an increase in the subtropical cell, and G is the term for the subtropical gyre, which is given by:

$$\frac{dG}{dt} = ET - KG + \gamma r2 \quad (5)$$

In (5), like in (2), E is an exchange coefficient, keeping temperature and the gyre related. ET and EG in our systems of equations represent exchanges between SST anomalies and the strength of the gyre, and the equilibrium temperature for SSTs is affected by the subtropical cell, which is also impacted by the gyre, keeping all three related. This can allow for irregular behavior, much like one sees with ENSO, and give a plausible physical explanation connecting

all of these. For more details and explanations of values of the constants, refer to section 4 of Farneti (2014).

When E is set to zero, leaving us with the classical delayed oscillator, we see very regular, QB behavior. When the exchange term is not zero however, allowing temperature to be affected by the subtropical gyre term, then we see more irregular behavior, with strong 4-7 year cycles, somewhat closer to what we see with ENSO, but still weaker than the biennial peak and the ~15 year peak. Even so, while the high amplitude in Farneti's model is somewhat higher than normally seen for ENSO, it still shows strong 4-7 year variability, which lines up reasonably well with ENSO's LF mode. Figure 10 also shows results for the strength of the subtropical gyre and cell, in the red and yellow lines, respectively.

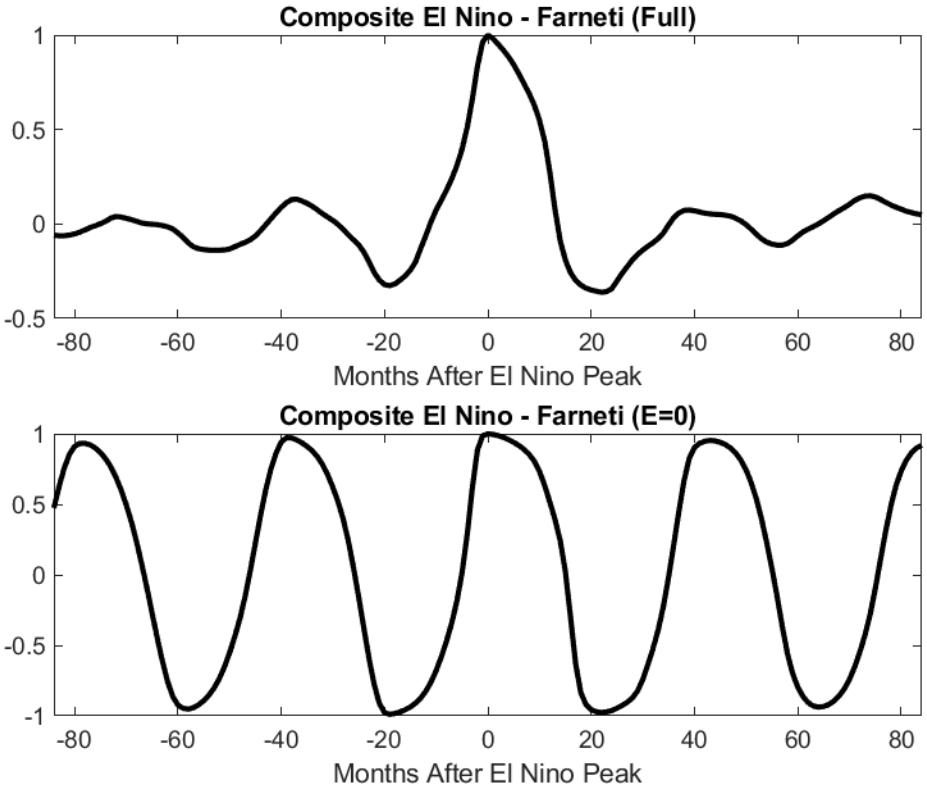

FIGURE 11: *Composite El Niño events from Farneti's (2014) full model (top), and with the exchange coefficient set to zero and logistic map set to a constant (bottom).*

Although there is too much QB variability in Farneti's full model thanks to its QB oscillator basis, the composite El Niño event based on this model's simulation looks much more like that of our observations (Fig. 11). When E is set to 0, the case in Figure 12, the composite El Niño event is extremely regular, with an equally strong La Niña about 20 months after the peak, and another El Niño peak ~40 months after. The peak in the spectrum at 3-4 years is consistent with the period inferred from the composite of 3-4 years when E=0. In the case of the full model, a weak, broad bump at ~40 months out and another centered around 70 months out is consistent with the power spectrum with broad peaks near 3–4 years and 5–7 years. Anything past a 7-year period on the power spectrum would not appear in composites, as these only include ±7 years around any given El Niño peak, so these composites would not show multidecadal variability, but are useful for QB and 4–7 year variability.

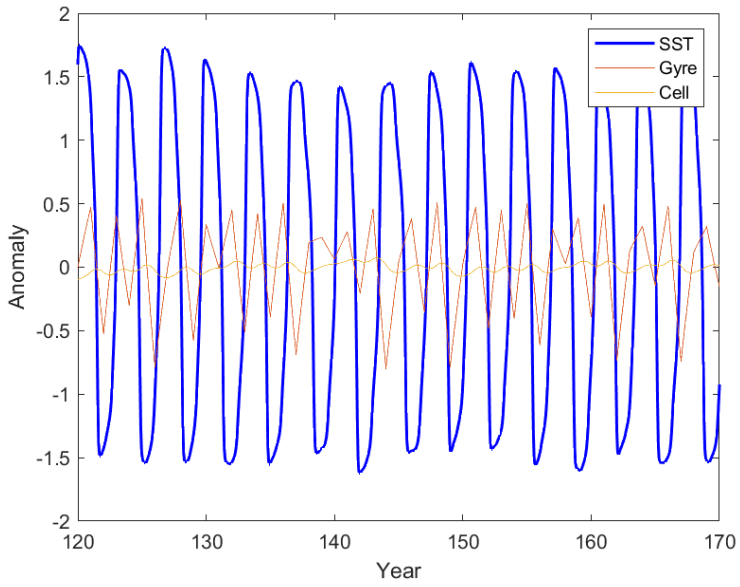

FIGURE 12: *The same as Fig 10, but with E=0, and the logistic map r1 set to constant. This is analogous to Figure 15 from Farneti (2014).*

With the exchange coefficient turned on, while we still have some hints of QB variability as we see in the observations, it is more muted, thanks to exchange terms increasing ENSO's irregularity and adding more periodicity at lower frequencies. The similarity of this model's composite with respect to the observed composite ENSO events suggests that this combination of the tropical delayed oscillator and the tropical-extratropical teleconnections via wind stress and the subtropical gyre/cell do a good job in explaining the behavior of the tropical Pacific around ENSO events.

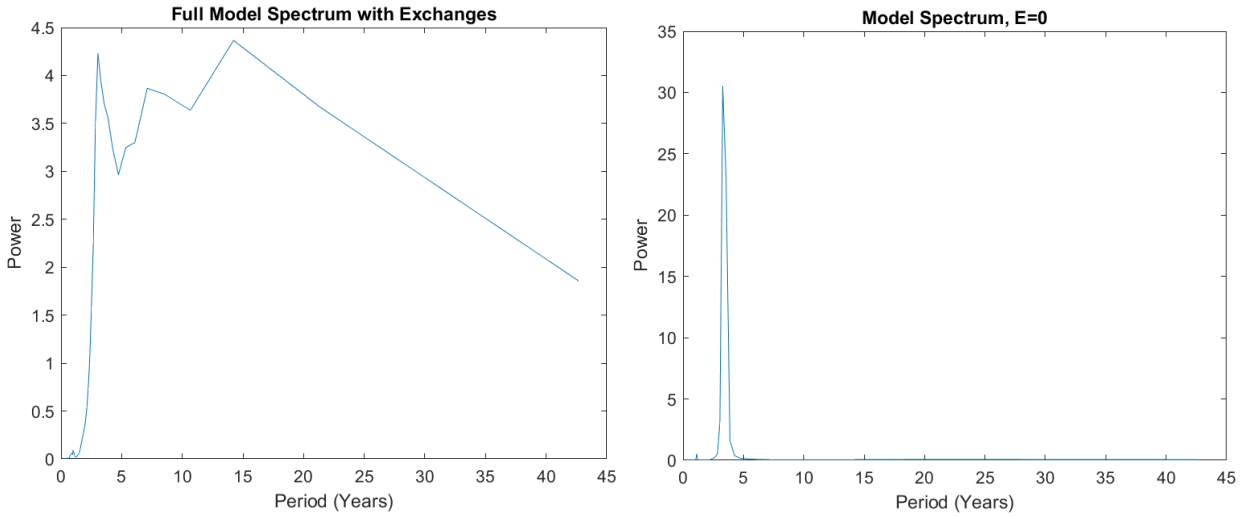

FIGURE 13: *Spectral power for both simulations, run 10,000 years for better resolution at low frequencies. The left figure shows the full model, with not just QB, but also LF and decadal variaibility, somewhat like what is observed with ENSO. The right shows the periodicity for the model with E=0 and r1 set to a constant, showing almost exclusively QB variaibility.*

This behavior of having more LF variability when the gyre exchange term is active and mainly having QB variability when the gyre exchange term is off is consistent with our hypothesis that QB variability is mainly from tropical processes, while the stronger LF variability is mainly from tropical-extratropical teleconnections.

7. Assessments of Global Climate Models

Finally, we wanted to see how well climate models deal with QB variability in ENSO in a few ways, so we performed the same analyses on CMIP5 data sets. In general, models made ENSO too regular, thus attributing too much variability to the QB frequencies. Figure 14 shows not only that the average model has too much variability, but also too much QB variability, causing some QBVARs to be almost double that of the OBS, and for the mean of the models, being a third too high.

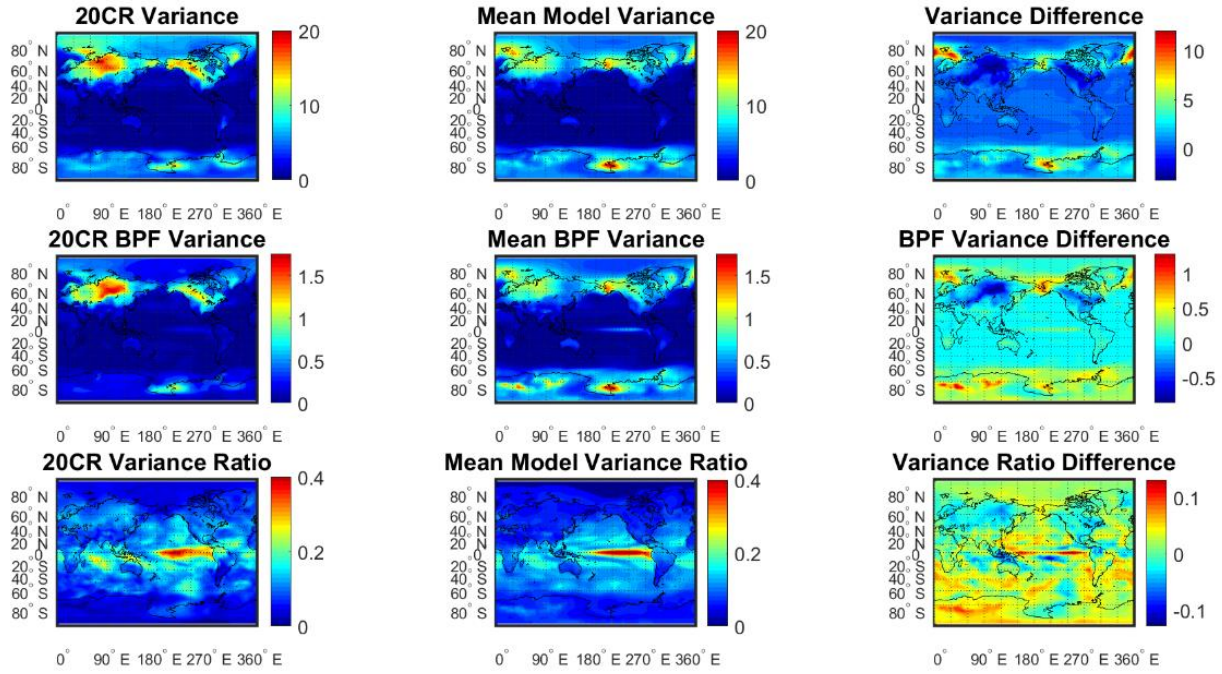

FIGURE 14: *Variance, QB variance, and the variance ratios for the average model, with these measures computed from the first ensemble member of each of 17 CMIP5 models, and then those 17 maps are averaged together. The difference between the mean model and the observations are in the right column.*

The QB variance ratios are too high in most global climate models, and this is mainly from the models being too regular in the QB range, as they have too much QB variance compared to the observations. However, the variance ratio being too high in the QB range may also have to do with LF variance being too low, as we see in the power spectra of several

models' realizations of the Niño 3.4 index (20th Centrury Reanalysis: Figure 15, models: Figures 16, 17). Jajcay et al (2018) found vast differences in ENSO between observations and models by several measures, and this study also finds differences between observed and simulated ENSO with different metrics as well. Many models make ENSO too regular, which we show not only in Figure 15, but also in composite ENSO events and power spectra in the appendix, with highlights in Figures 16 and 17.

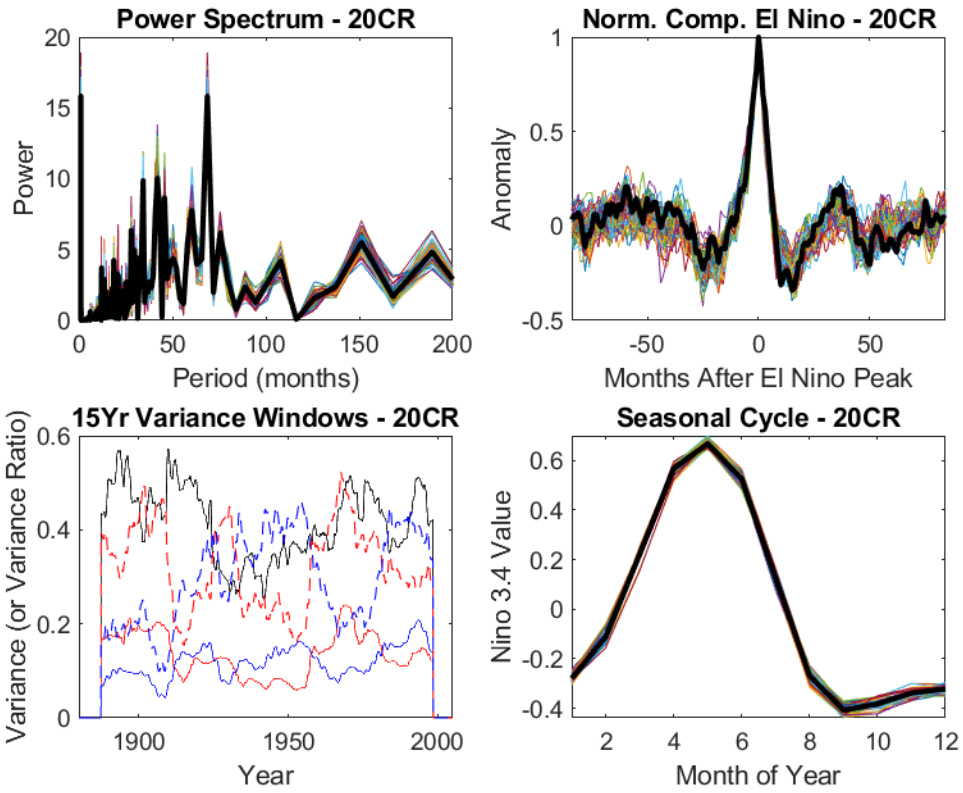

FIGURE 15: *Power spectrum (top left), normalized composite El Niño event (top right), 15 year variance windows (bottom left), and the seasonal cycle of the Niño 3.4 index from the 20th Century Reanalysis.*

Some models are far too consistent and regular in QB behavior. 20CR's composite suggest that there is usually a negative ENSO value before and after an ENSO peak, though negative does not need to be strong enough to be a La Niña event. For global climate models to

handle ENSO correctly, they should have this pattern, However, some models have a far too regular pattern, with a definite La Niña event following or preceding the El Niño peak. Other models have the opposite extreme, where there seems to be no predictability past a few months. The models that handle this QB behavior are also the ones that handle other aspects of ENSO the best, suggesting the importance of QB variability in ENSO, such as seasonal cycles, which are in the appendix as they are not the focus of this study.

While the appendix shows the power spectrum, composite El Niño, variance windows, and seasonal cycles for the Niño 3.4 index for each of the 17 GCMs investigated here, Figure 15 shows these from 20CR. Figures 16 and 17 show these for two climate models, and the results for the rest of the models generally look like one of these, and can be found in the appendix.

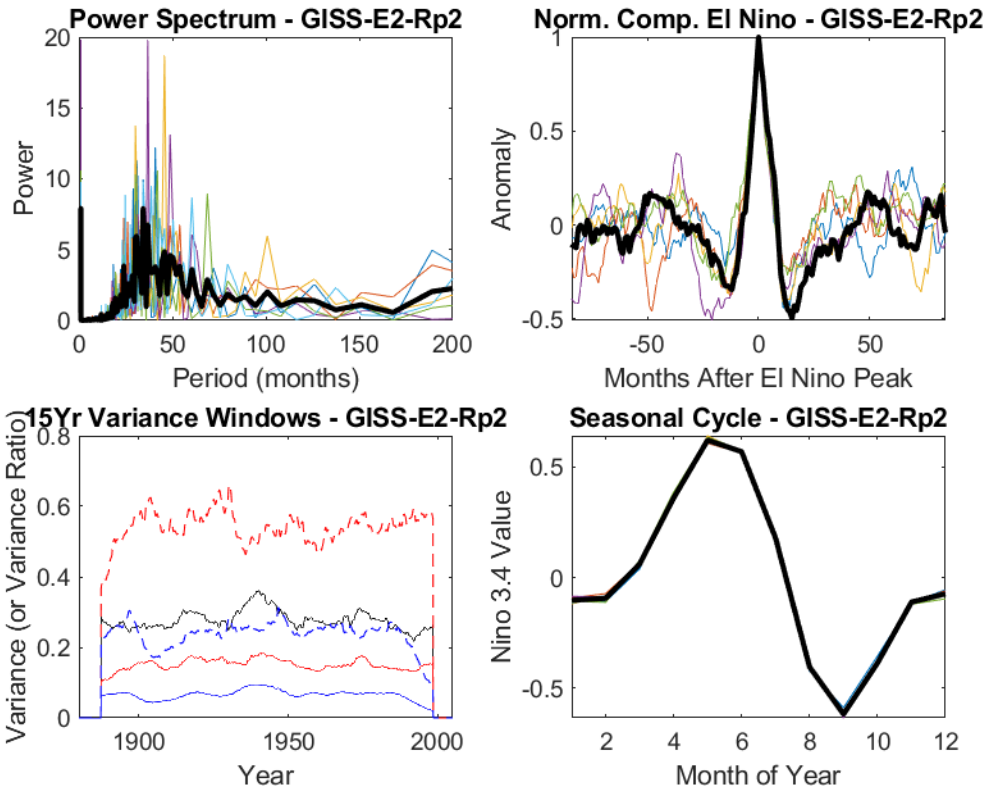

FIGURE 16: *The same analyses as in Figure 15, but for the GISS-E2-Rp2 global climate model.*

The GISS-E2-Rp2 model handles several aspects of the Niño 3.4 index reasonably well, though still has issues (Fig. 16). Its power spectrum has somewhat higher power in the QB range than in the LF range, where there is a peak near 30-40 months, higher than a broad peak centered around 50 months, and we can see this heightened QB power in the composite El Niño. On average, this model expects a weak La Niña 1-2 years after an El Niño peak, falling to -0.5, instead of -0.3 in the reanalysis. Still, it exhibits similar behavior to the observed composite, moving back up to zero around 4 years before or after an event. An overestimate of QB variability holds this - and several models - back when we see the 15-year variance windows. In this model, the red lines, representing the variance from QB (18-42 month) bandpass-filtered data, are consistently above the blue lines, representing the LF (42-84 month) filtered data. In the observations, these switch back and forth over decades.

This variance window panel tells us two things. First, this model overestimates QB variability, making its ENSO somewhat too regular. Additionally, it underestimates decadal and multidecadal variability, which we can see in the power spectrum. 10 out of 17 models we investigated consistently had the 18-42 month variance be greater than 42-84 month variance for the whole model run. These were all 6 GISS models, CNRM-CM5, GFDL-CM3, HadCM3, and MIROC5. Of the remaining 7, all of them switched back and forth at least once, and although 10 of 17 consistently had more QB than LF variability for the whole run, none ever consistently had more LF than QB variability.

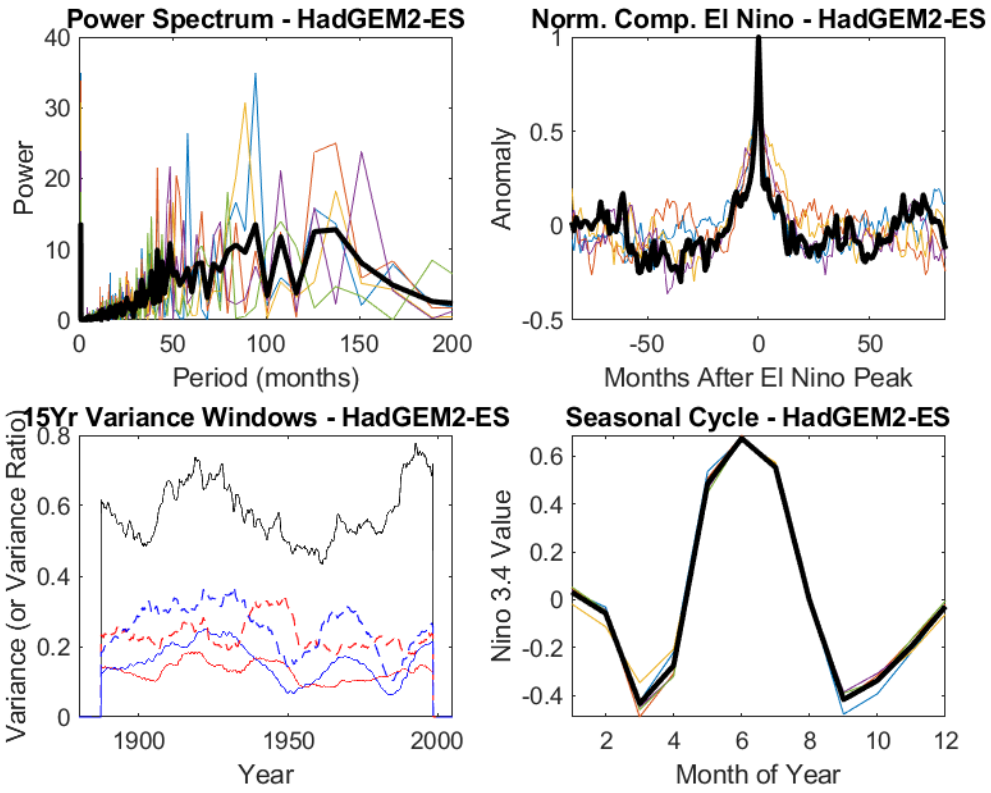

FIGURE 17: *The same as Figures 15 and 16, but for the HadGEM2-ES model.*

The GISS models are examples of models that overestimated QB variability. However, other models, such as the HadGEM2-ES underestimated it and/or overestimated LF and decadal variability (Fig. 17). While in observations, there is a weak but noticeable fall to -0.3 or so 1-2 years after an El Niño peak, the HadGEM2-ES does not exhibit much of this behavior at all, falling towards zero and staying around there more than one year away from a peak. While most models with too much QB variability had too deep a trough, this hardly has one at all, with only broad but shallow troughs on average, and this is not even consistent among ensemble members. Additionally, it also struggles with the seasonal cycle somewhat. In observations (Fig 15), the Niño 3.4 index peaks in April-June, with its lowest values in the fall, climbing through winter and spring. This model's seasonal peak is in June, which is reasonable, but it has two troughs

curiously, in September, which is similar to when the observed seasonal cycle falls, but also in March, when observed ENSO is already rising sharply. However, it does have the correct amplitude for the seasonal cycle, with a maximum near 0.6, and a minimum near -0.4.

Other models, even ones that switch between LF and QB playing a larger role, with results shown in the appendix, struggle with amplitude. Of these remaining 7 with variance windows that switched back and forth, five of them struggled in some way with the seasonal cycle. MRI-CGCM3 struggled severely with timing of the seasonal cycle, so while it had a comparable amplitude to that of observations, its peak was incorrectly in December instead of May. The seasonal cycle from HadGEM2-ES has already been analyzed, leaving us with five models not discussed yet.

Of these five models, the CanESM2, CSIRO-360, and GFDL-CM2p1 all have too high amplitudes for the seasonal cycle, 1.5-2 times that of observations, though the timing is fine. This leaves us with the CCSM4 and IPSL-CM5A-LR models as the best with respect to variance windows and the seasonal cycle. CCSM4 usually has variance of 0.8 in each 15 year period, higher than the ~0.5 observed, though IPSL handles this accurately, leaving it as the best by these four metrics. Even so, this model has issues as well, as discussed in Jacjay et al. (2018). Still, while the IPSL has slightly too strong troughs after an El Niño event, and slightly too much QB power in its power spectrum, it exhibits close composites to observations compared to most other models, suggesting that the correct balance and mechanisms behind QB variability and LF variability would vastly help in predicting and handling of ENSO events. Models with too much QB variability make ENSO too regular, but models with too much LF and decadal variability make it too irregular. While the IPSL handles ENSO reasonably well by these four metrics, it still could be improved; every model has some flaws with ENSO, most overestimate QB

variability, and some do not even have the right seasonal cycle, indicating serious underlying issues in how they handle processes governing tropical oceans and ENSO.

8. Summary and Conclusion

While more of ENSO's periodicity is in the LF range than the QB range, defined in this study as approximately 18-42 months, the QB range still plays an important role. In composite El Niño events, QB variability is evident according to each ensemble member of the 20th Century Reanalysis. This supports investigations of QB variability, and this range is in line with the period from the classical delayed oscillator model by Suarez and Schopf (1988). QB variability can be mapped by putting observations through a simple bandpass filter after removing the seasonal cycle, and then taking the variance at each point. This can be compared to the full temperature anomaly map, again after removing the seasonal cycle, to show global maps of temperature variability, QB variability, and the QB variance ratio.

The QB variance ratio is higher in the tropics than higher latitudes, and higher over oceans than land, while overall, QBVARs are highest in the tropical Pacific, again suggesting the QB variability plays a major role in ENSO. Discriminant analysis reveals that there is only one consistently strong mode that is confined within the tropics on the QB timescale, which tells us that QB variability can be explained mainly by tropical processes. A second pattern had some connection to the midlatitudes, but generally was quite weak in the tropics in the QB range, suggesting that any connection to the midlatitudes, were it important for ENSO, would be strongest in another frequency band. The delayed oscillator model would potentially work as this one tropical QB mode, being based on equatorial waves, and oscillating approximately every

three years. This alone would not explain ENSO's irregularity, nor does it explain ENSO's high spectral power in the LF range or beyond, so for those, other mechanisms must be investigated.

Over time, the QB mode and the LF mode strengthen and weaken, both in their absolute variance, and in their variance ratios with respect to that of ENSO, with some decades having more of one than the other, suggesting decadal and multidecadal variability playing a role to modulate the strength of both of these modes. A system of three ordinary differential equations connects these themes together by connecting tropical SSTs and thus ENSO to the subtropical gyre and subtropical cell of the North Pacific, via wind stress. This system of equations by Farneti et al (2014) produces a power spectrum more like that of ENSO than the CMIP5 global climate models produce. It builds on the delayed oscillator and thus has almost exclusively QB variability when exchange terms are turned off, and has QB, LF, and decadal variability when exchanges between the tropics and subtropical circulations are included.

CMIP5 models generally have too much variability in the tropical Pacific in the QB range, as well as too high a QBVAR in that region as well, going along with findings from Jajcay et al. (2018) that most models struggle with ENSO and make it too regular. Additionally, GCMs having too much QB variability specifically in the tropics suggests goes along with the hypothesis that QB ENSO variability is mainly tropical.

The results of this study, along with previous work along the lines of Suarez and Schopf (1988) and Farneti et al. (2014)suggest that QB variations in ENSO are primarily from tropical mechanisms, likely the delayed oscillator, and that LF variations are from tropical-extratropical teleconnections, specifically via tropical SST anomalies leading to wind stress anomalies in the subtropical Pacific, thus affecting the subtropical gyre and subtropical cell, and in turn, SSTs.

9. Future Work

As much as climate models have improved in recent years, there is still work to be done in improving their handling of ENSO. As the variance errors in the arctic, there are still some issues to work out with ocean currents and extratropical teleconnections in general, and as Farneti's findings suggest, these could lead to great improvements in Pacific temperature variability.

Applying variance ratios to other frequency bands and to different data sets either for ENSO or other parts of the ocean-atmosphere system may prove insightful for learning about processes in various timescales not focused on much yet. Of course, longer data sets would be better, especially for lower frequencies.

Farneti's model is likely a good basis, which in turn is based on the delayed oscillator by Suarez and Schopf (1988), seems to be a good basis for a more predictive ENSO model. Of course, the gyre and cell terms are idealized, so scaling these simple terms to real physical parameters for vast circulations could be challenging. Even so, including tropical-extratropical teleconnections and a seasonal forcing on top of the classical oscillator would likely be quite useful in simulating ENSO even more effectively.

Finally, more observations would prove quite useful. This study only used surface temperature data, though much of ENSO's variability involves hundreds of meters of depth into the ocean as the thermocline and currents change. Additionally, our observations even at the ocean surface are rather sparse. With more observations, we can achieve better understanding not just of ENSO, but of the whole world's climate variability affected by it.

References

Bejarano, L., and F.-F. Jin, 2008: Coexistence of equatorial coupled modes of ENSO. *J. Climate*, **21**, 3051–3067, https://doi.org/10.1175/2007JCLI1679.1.

Bjerknes, J., 1969: Atmospheric Teleconnections from the Equatorial Pacific. *Mon. Wea. Rev.* (1969) **97** (3): 163–172, https://doi.org/10.1175/1520-0493(1969)097<0163:ATFTEP>2.3.CO;2

Capotondi, A., and coauthors, 2015: Understanding ENSO Diversity. *Bull. Amer. Meteor. Soc.* (2015) **96** (6): 921–938, https://doi.org/10.1175/BAMS-D-13-00117.1

Deser, C., and coauthors, 2017: The Northern Hemisphere Extratropical Atmospheric Circulation Response to ENSO: How Well Do We Know It and How Do We Evaluate Models Accordingly? *J. Climate* (2017) **30** (13): 5059–5082, https://doi.org/10.1175/JCLI-D-16-0844.1

Ding, R., J. Li, Y.-h. Tseng, C. Sun, and Y. Guo, 2015: The Victoria mode in the North Pacific linking extratropical sea level pressure variations to ENSO. *J. Geophys. Res. Atmos.*,120, 27–45, doi:10.1002/2014JD022221.

Farneti, R., F. Molteni, and F. Kucharski, 2014: Pacific interdecadal variability driven by tropical-extratropical interactions. *Clim. Dyn.* (2014) 42: 3337-3355 DOI: 10.1007/s00382-013-1906-6

Furtado, J., and coauthors, 2012: Linkages between the North Pacific Oscillation and central Pacific SSTs at low frequencies. *Clim. Dyn.* (2012) 39: 2833-2846, DOI: 10.1007/s00382-011-1245-4

Jajcay, N., S. Kravtsov, G. Sugihara, A. Tsonis, and M. Palus, 2018: Synchronization and causality across time scales in El Niño Southern Oscillation. *Climate and Atmospheric Science* (2018) 33. https://www.nature.com/articles/s41612-018-0043-7

Jin, F.-F., D. Neelin, and M. Ghil, 1994: El Niño on the Devil's Staircase: Annual Subharmonic Steps to Chaos. *Science,* New Series, Vol. 264, No. 5155 (Apr. 1, 1994), 70-72. DOI: 10.1126/science.264.5155.70

Kravtsov, S., 2017: Pronounced differences between observed and CMIP5-simulated multidecadal climate variability in the twentieth century. *Geophysical Research Letters,* (2017) **44** (11): 5749-5757, https://doi.org/10.1002/2017GL074016

Kravtsov, S., and D. Callicutt, 2017: On semi-empirical decomposition of multidecadal climate variability into forced and internally generated components. *International Journal of Climatology*, (2017) **37** (12): 4417-4433, https://doi.org/10.1002/joc.5096

Kravtsov, S., C. Grimm, and S. Gu, 2018: Global-scale multidecadal variability missing in state-of-the-art climate models. *npj Clim Atmos Sci* **1,** 34 (2018). https://doi.org/10.1038/s41612-018-0044-6

Neelin, J. D, 1991: The Slow Sea Surface Temperature Mode and the Fast-Wave Limit: Analytic Theory for Tropical Interannual Oscillations and Experiments in a Hybrid Coupled Model. *J. Atm. Sci.*, **48** (4): 584-606, https://doi.org/10.1175/1520-0469(1991)048%3C0584:TSSSTM%3E2.0.CO;2

Schneider, T. and I. Held, 2001: Discriminants of Twentieth-Century Changes in Earth Surface Temperatures. *J. Cli.* (2001) **14** (3): 249-254, https://doi.org/10.1175/1520-0442(2001)014%3C0249:LDOTCC%3E2.0.CO;2

Suarez, M., and P. Schopf. 1988: A Delayed Action Oscillator for ENSO. *J. Atmos. Sci.* (1988) **45** (21): 3283–3287, https://doi.org/10.1175/1520-0469(1988)045%3C3283:ADAOFE%3E2.0.CO;2

Taylor, K., R. Stouffer, and G. Meehl., 2012: An Overview of CMIP5 and the Experiment Design. *Bull. Amer. Meteor. Soc.* (2012) **93** (4): 485-498, https://doi.org/10.1175/BAMS-D-11-00094.1

Walker, G., 1926: Correlation in Seasonal Variations of Weather, IX: A Further Study of World Weather. *Memoirs of the India Meteorological Department* (1922-25). **XXIV**: 274-333, https://www.rmets.org/sites/default/files/classicindia2.pdf

Wang, R., and H.-L. Ren, 2020: Understanding Key Roles of Two ENSO Modes in Spatiotemporal Diversity of ENSO. *J. Cli.* (2020) **33** (15): 6453-6469. https://doi.org/10.1175/JCLI-D-19-0770.1

Wyrtki, K., 1975: El Niño – The Dynamic Response of the Equatorial Pacific Ocean to Atmospheric Forcing. *J. Phys. Oceanogr.* (1975) **5** (4): 572-584. https://doi.org/10.1175/1520-0485(1975)005%3C0572:ENTDRO%3E2.0.CO;2

Xie, F., and coauthors, 2014: A connection from Arctic stratospheric ozone to El Niño-Southern Oscillation. *Environ. Res. Lett.* **11** 124026

Appendix: ENSO Statistics from CMIP5 Models

The following figures show four panels of data for realizations of the Niño 3.4 index from each of 17 CMIP5 models, as well as the 20th Century Reanalysis. The top left panel shows the power spectrum. The top right panel shows the power spectrum, as in Figure 1; the top right shows composite El Niño time series events, as in Figure 2; the bottom left shows 15 year variance windows, with the same calculations and color scheme as in Figure 6; the bottom right shows the seasonal cycle of the index. In each panel that shows ensemble members, the average properties of each are shows in a bold, black line, while each ensemble member is measured with a thin colorful line.

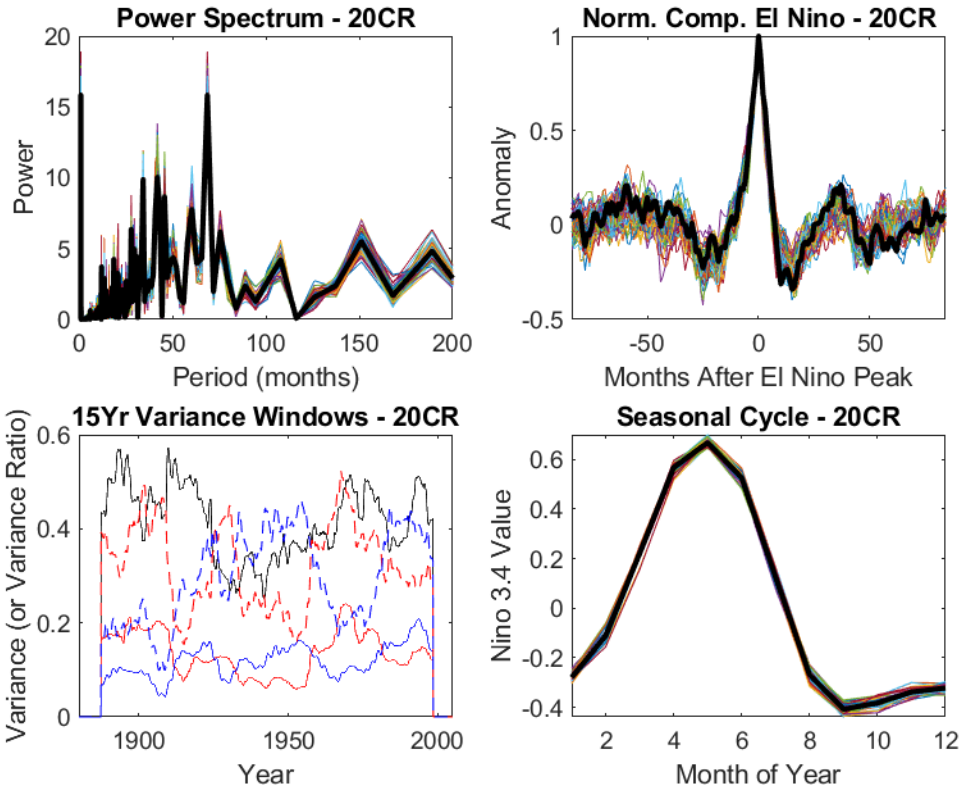

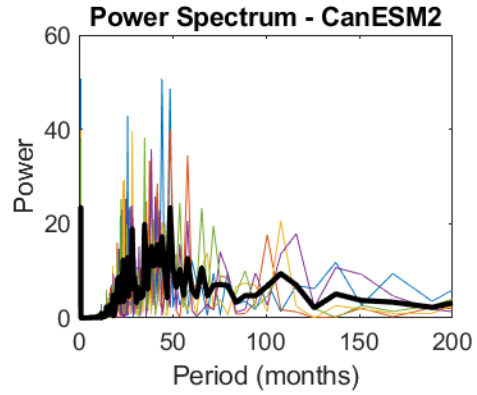
Power Spectrum - CanESM2
Power
Period (months)
0
20
40
60
0
50
100
150
200

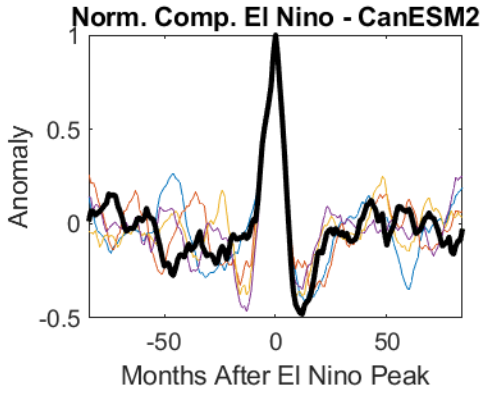
Norm. Comp. El Nino - CanESM2
Anomaly
Months After El Nino Peak
-0.5
0
0.5
1
-50
0
50

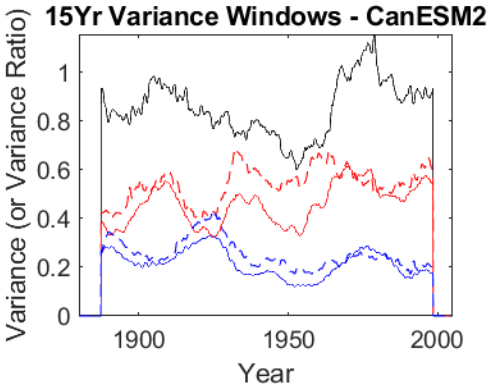
15Yr Variance Windows - CanESM2
Variance (or Variance Ratio)
Year
0
0.2
0.4
0.6
0.8
1
1900
1950
2000

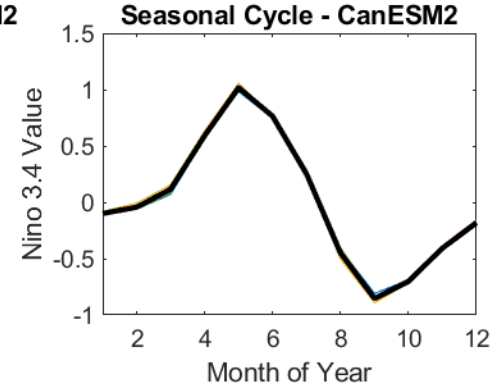
Seasonal Cycle - CanESM2
Nino 3.4 Value
Month of Year
-1
-0.5
0
0.5
1
1.5
2
4
6
8
10
12

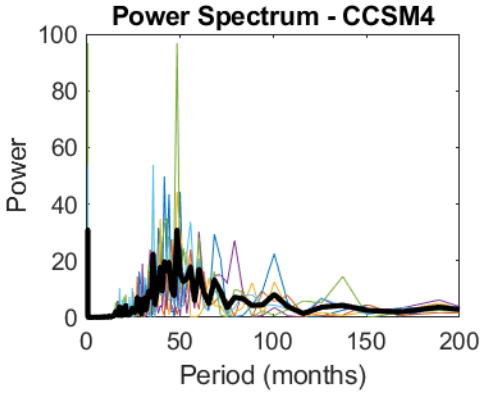
Power Spectrum - CCSM4
Power
Period (months)
0
20
40
60
80
100
0
50
100
150
200

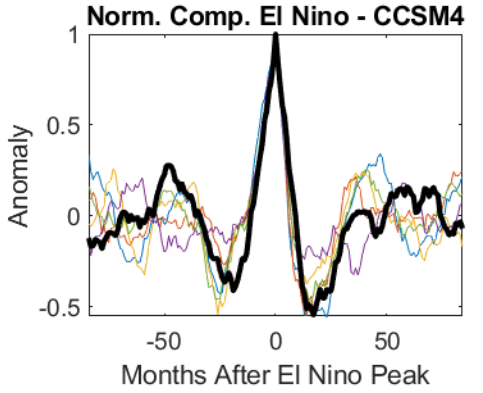
Norm. Comp. El Nino - CCSM4
Anomaly
Months After El Nino Peak
-0.5
0
0.5
1
-50
0
50

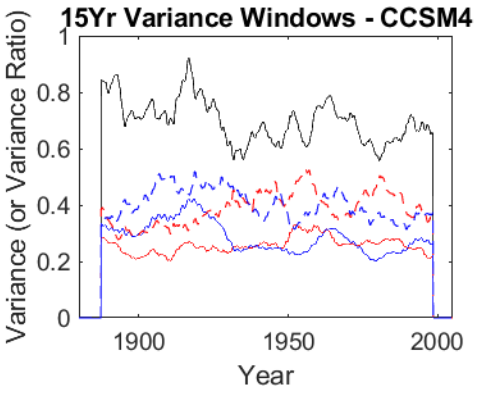
15Yr Variance Windows - CCSM4
Variance (or Variance Ratio)
Year
0
0.2
0.4
0.6
0.8
1
1900
1950
2000

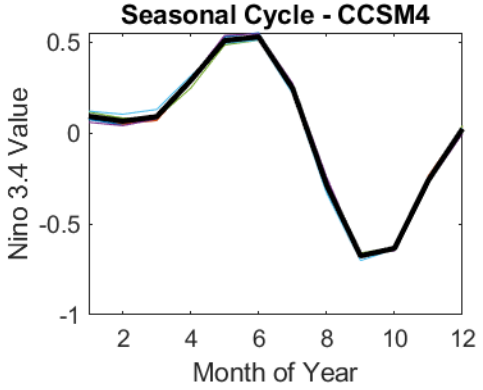
Seasonal Cycle - CCSM4
Nino 3.4 Value
Month of Year
-1
-0.5
0
0.5
2
4
6
8
10
12

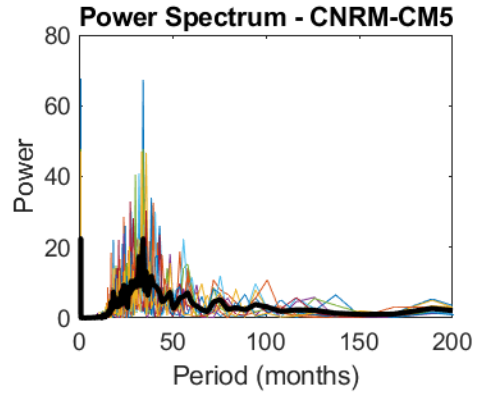
Power Spectrum - CNRM-CM5
Power
Period (months)

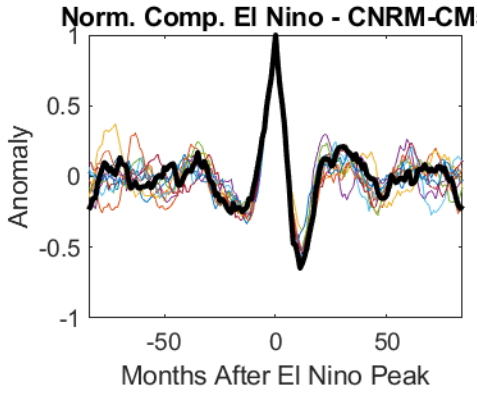
Norm. Comp. El Nino - CNRM-CM5
Anomaly
Months After El Nino Peak

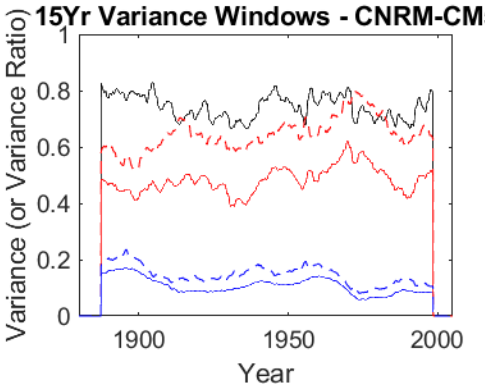
15Yr Variance Windows - CNRM-CM5
Variance (or Variance Ratio)
Year

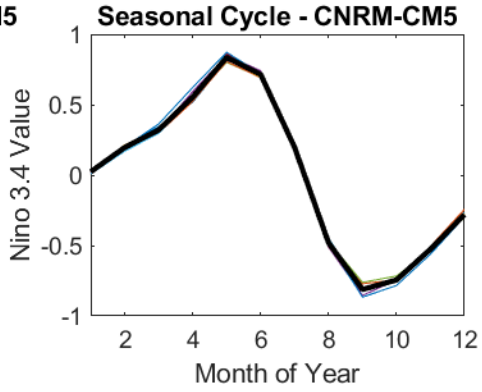
Seasonal Cycle - CNRM-CM5
Nino 3.4 Value
Month of Year

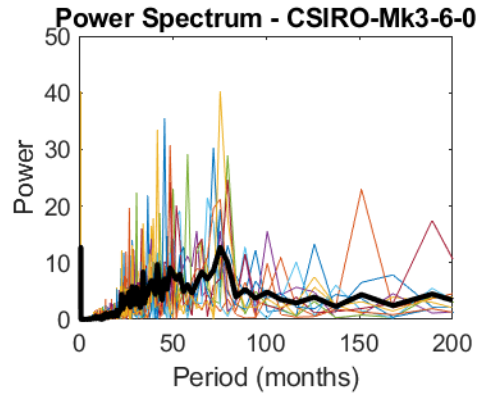
Power Spectrum - CSIRO-Mk3-6-0
Power
Period (months)

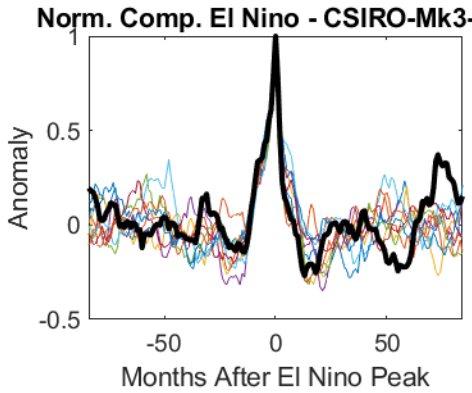
Norm. Comp. El Nino - CSIRO-Mk3-6-0
Anomaly
Months After El Nino Peak

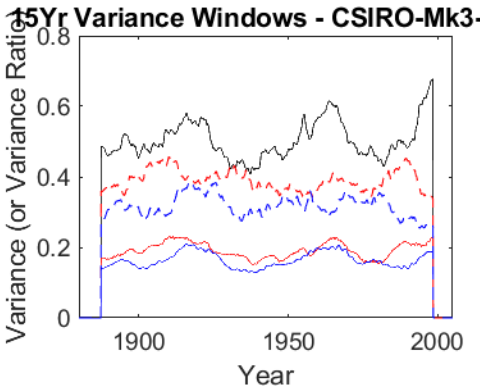
15Yr Variance Windows - CSIRO-Mk3-6-0
Variance (or Variance Ratio)
Year

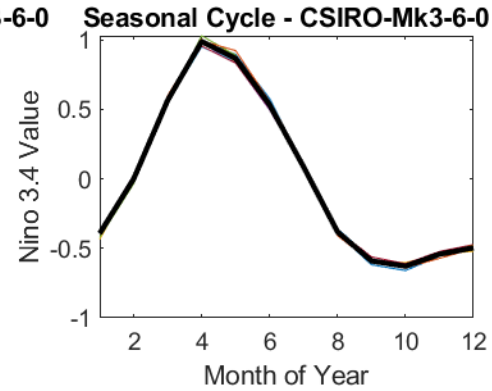
Seasonal Cycle - CSIRO-Mk3-6-0
Nino 3.4 Value
Month of Year

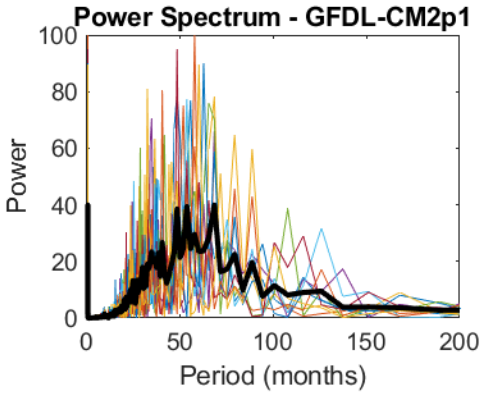
Power Spectrum - GFDL-CM2p1
Power
Period (months)

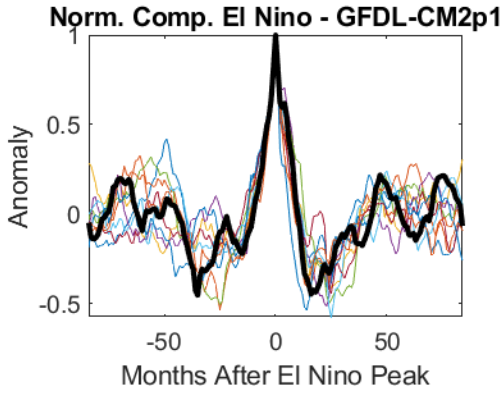
Norm. Comp. El Nino - GFDL-CM2p1
Anomaly
Months After El Nino Peak

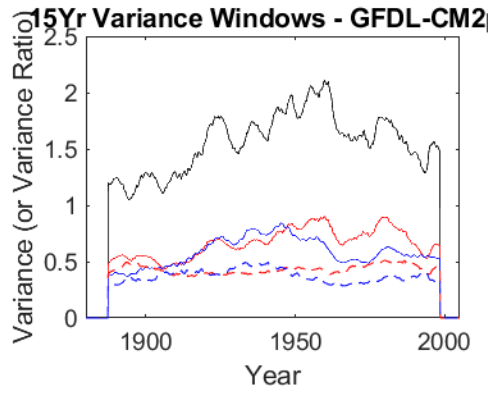
15Yr Variance Windows - GFDL-CM2p1
Variance (or Variance Ratio)
Year

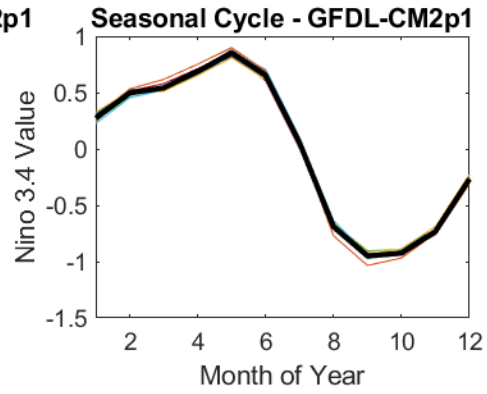
Seasonal Cycle - GFDL-CM2p1
Nino 3.4 Value
Month of Year

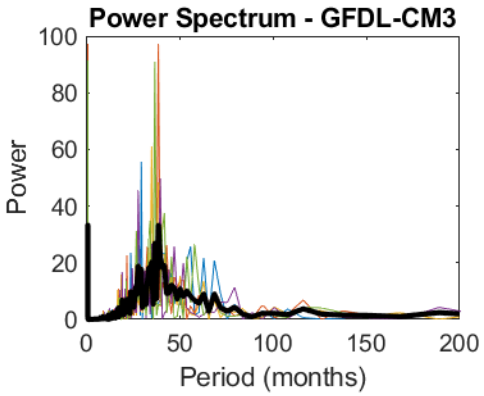
Power Spectrum - GFDL-CM3
Power
Period (months)

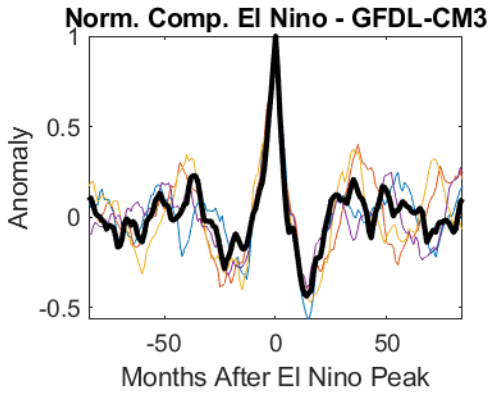
Norm. Comp. El Nino - GFDL-CM3
Anomaly
Months After El Nino Peak

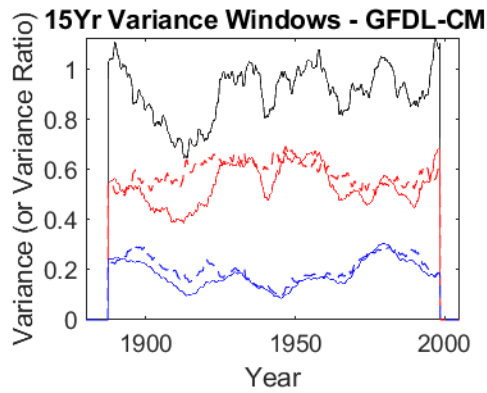
15Yr Variance Windows - GFDL-CM3
Variance (or Variance Ratio)
Year

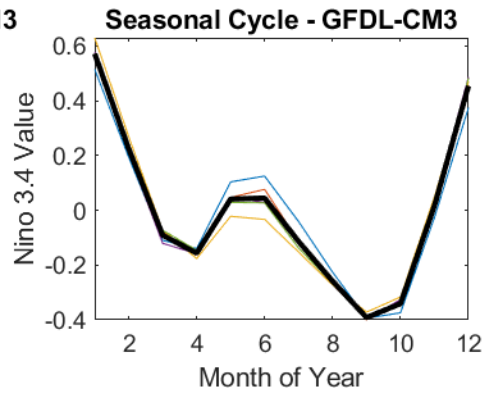
Seasonal Cycle - GFDL-CM3
Nino 3.4 Value
Month of Year

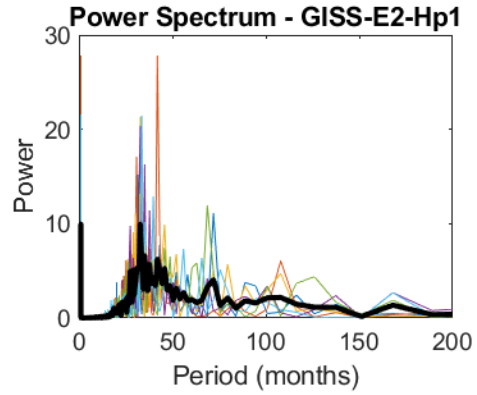
Power Spectrum - GISS-E2-Hp1
Power
Period (months)

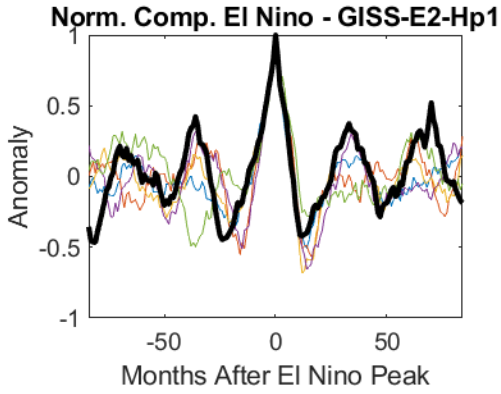
Norm. Comp. El Nino - GISS-E2-Hp1
Anomaly
Months After El Nino Peak

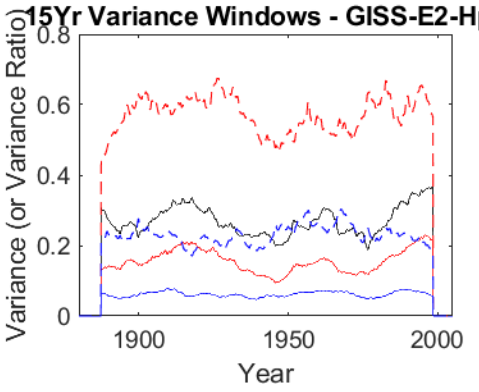
15Yr Variance Windows - GISS-E2-Hp1
Variance (or Variance Ratio)
Year

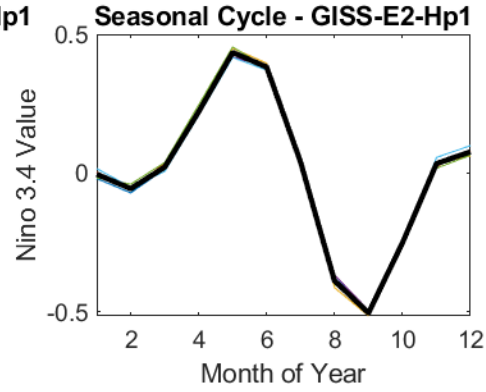
Seasonal Cycle - GISS-E2-Hp1
Nino 3.4 Value
Month of Year

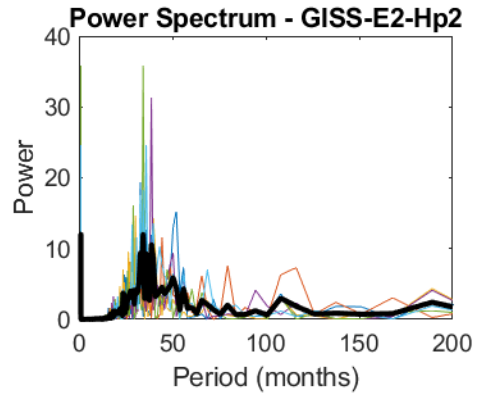
Power Spectrum - GISS-E2-Hp2
Power
Period (months)

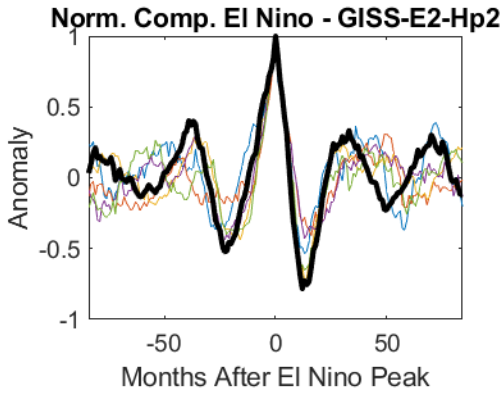
Norm. Comp. El Nino - GISS-E2-Hp2
Anomaly
Months After El Nino Peak

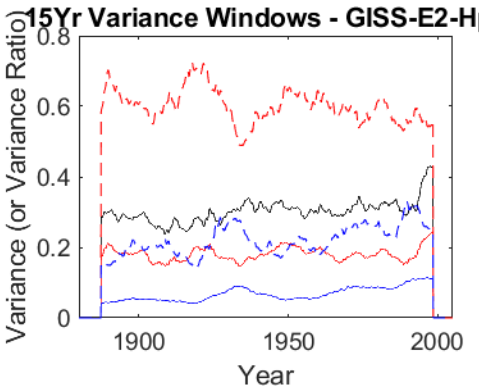
15Yr Variance Windows - GISS-E2-Hp2
Variance (or Variance Ratio)
Year

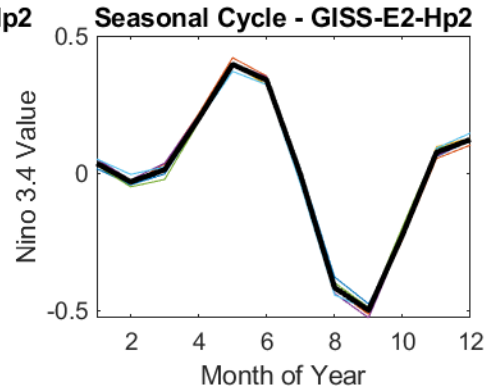
Seasonal Cycle - GISS-E2-Hp2
Nino 3.4 Value
Month of Year

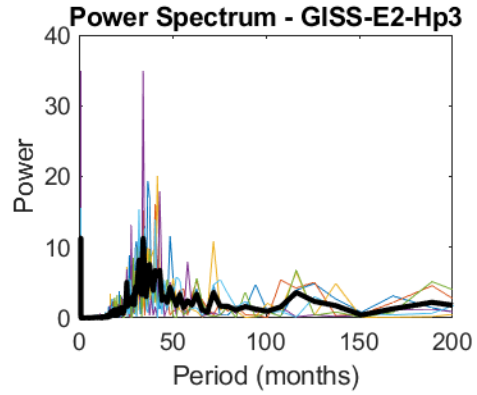
Power Spectrum - GISS-E2-Hp3
Power
Period (months)

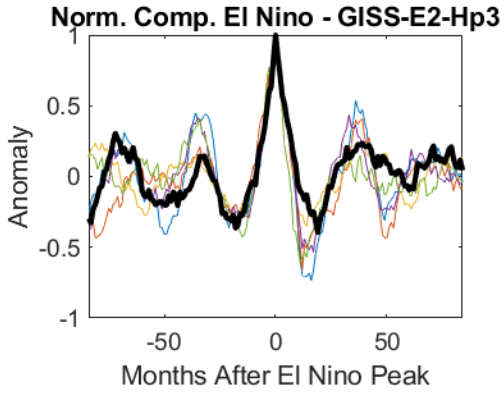
Norm. Comp. El Nino - GISS-E2-Hp3
Anomaly
Months After El Nino Peak

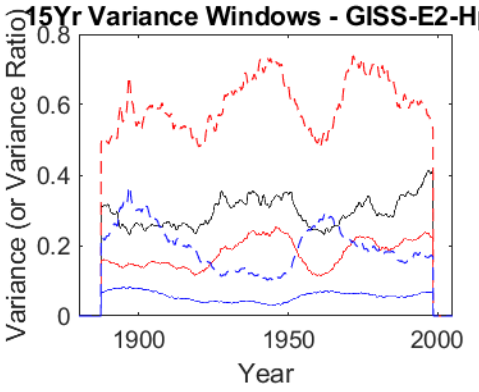
15Yr Variance Windows - GISS-E2-Hp3
Variance (or Variance Ratio)
Year

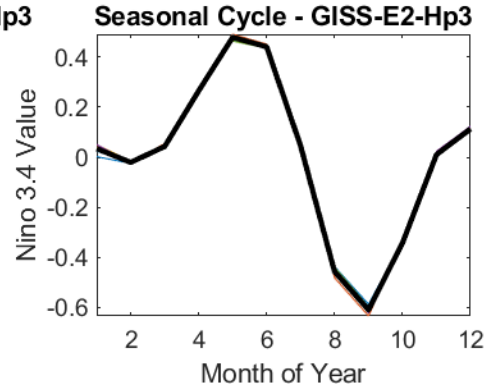
Seasonal Cycle - GISS-E2-Hp3
Nino 3.4 Value
Month of Year

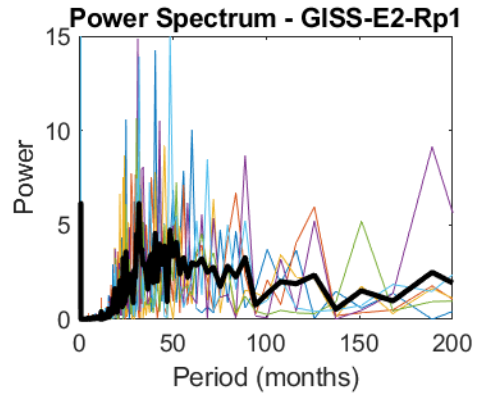
Power Spectrum - GISS-E2-Rp1
Power
Period (months)

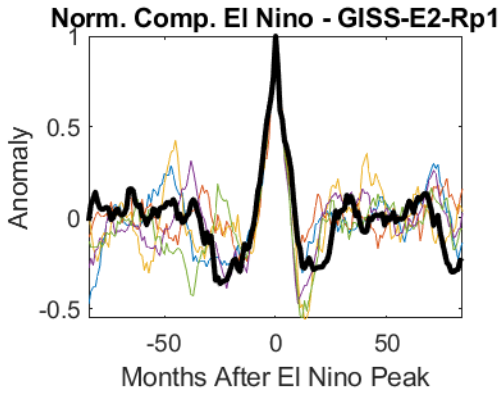
Norm. Comp. El Nino - GISS-E2-Rp1
Anomaly
Months After El Nino Peak

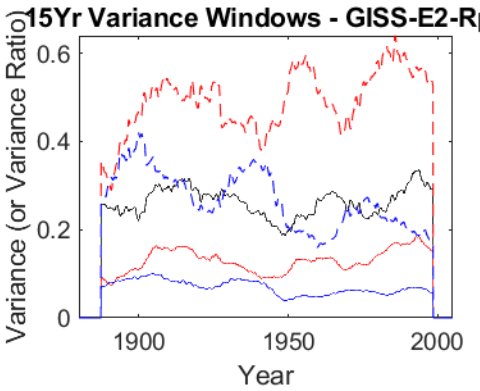
15Yr Variance Windows - GISS-E2-Rp1
Variance (or Variance Ratio)
Year

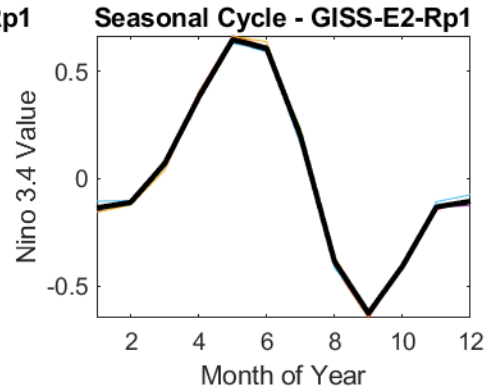
Seasonal Cycle - GISS-E2-Rp1
Nino 3.4 Value
Month of Year

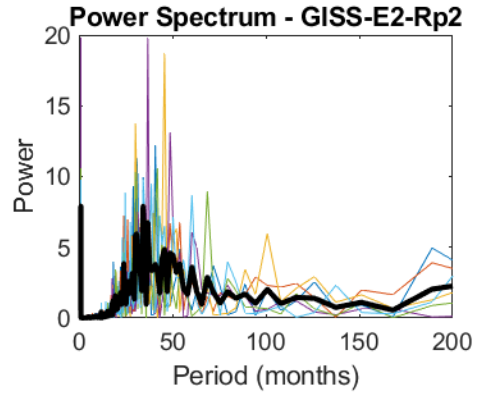
Power Spectrum - GISS-E2-Rp2
Power
Period (months)

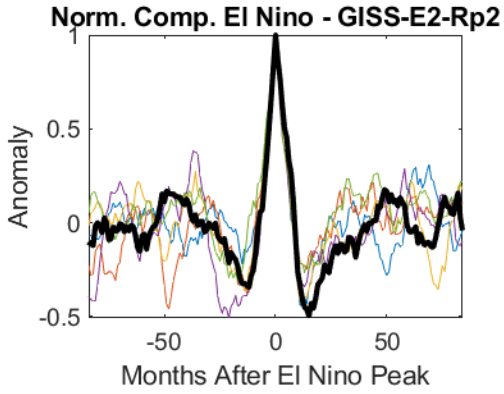
Norm. Comp. El Nino - GISS-E2-Rp2
Anomaly
Months After El Nino Peak

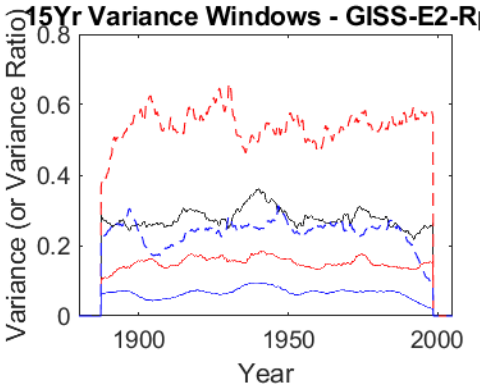
15Yr Variance Windows - GISS-E2-Rp2
Variance (or Variance Ratio)
Year

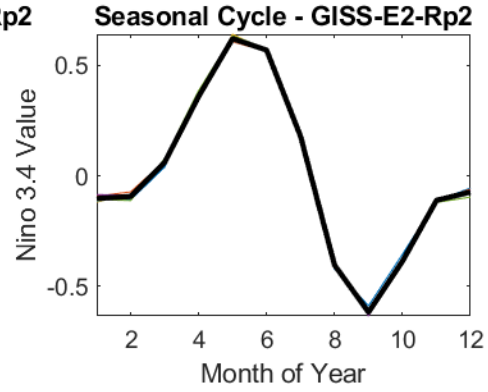
Seasonal Cycle - GISS-E2-Rp2
Nino 3.4 Value
Month of Year

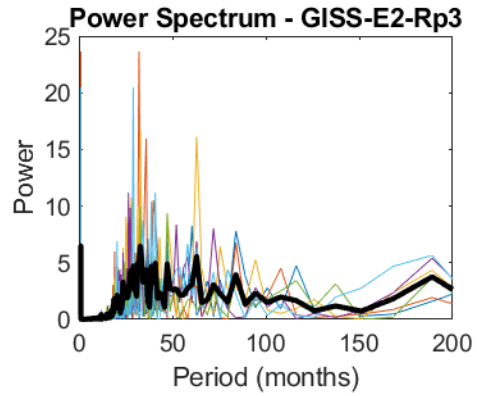
Power Spectrum - GISS-E2-Rp3
Power
Period (months)

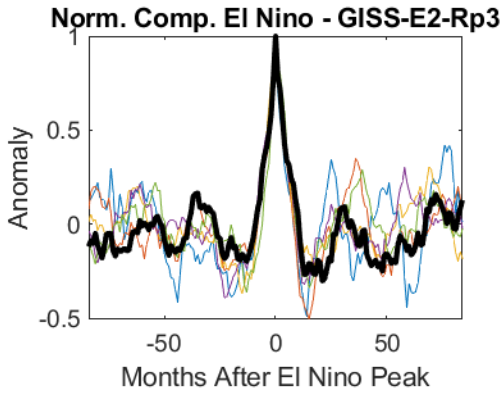
Norm. Comp. El Nino - GISS-E2-Rp3
Anomaly
Months After El Nino Peak

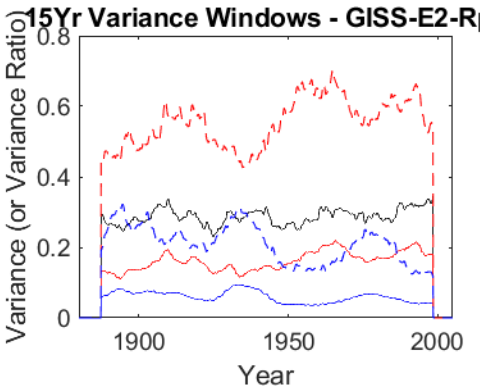
15Yr Variance Windows - GISS-E2-Rp3
Variance (or Variance Ratio)
Year

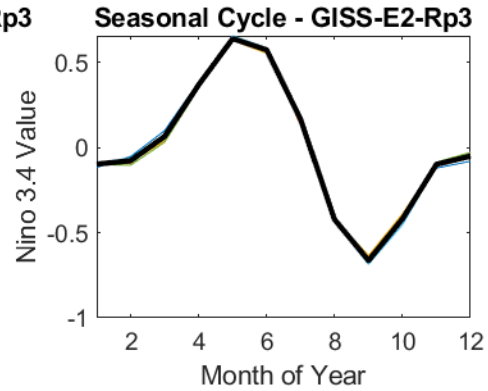
Seasonal Cycle - GISS-E2-Rp3
Nino 3.4 Value
Month of Year

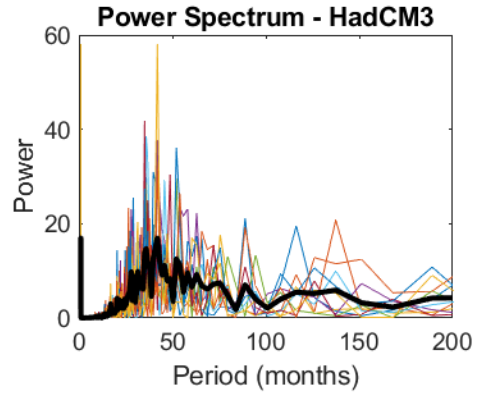
Power Spectrum - HadCM3
Power
Period (months)
0
20
40
60
0
50
100
150
200

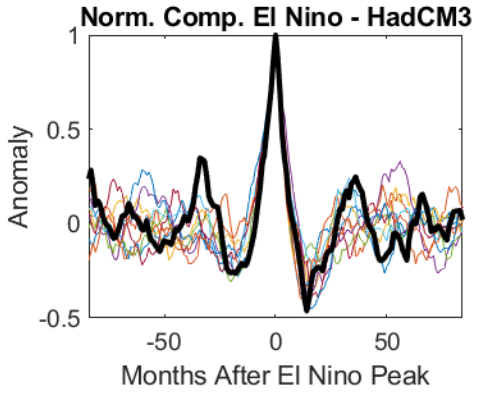
Norm. Comp. El Nino - HadCM3
Anomaly
Months After El Nino Peak
-0.5
0
0.5
1
-50
0
50

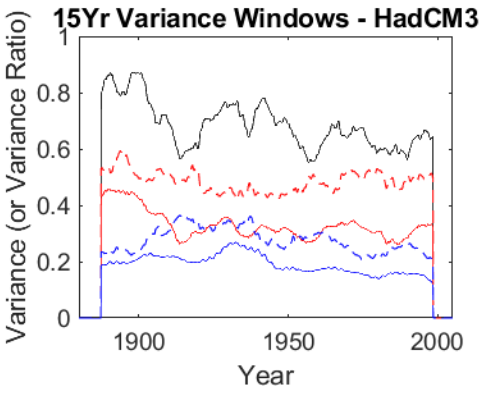
15Yr Variance Windows - HadCM3
Variance (or Variance Ratio)
Year
0
0.2
0.4
0.6
0.8
1
1900
1950
2000

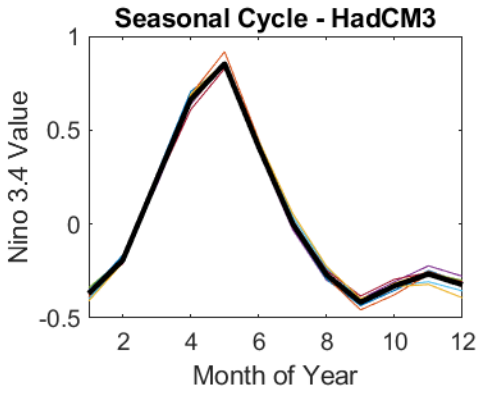
Seasonal Cycle - HadCM3
Nino 3.4 Value
Month of Year
-0.5
0
0.5
1
2
4
6
8
10
12

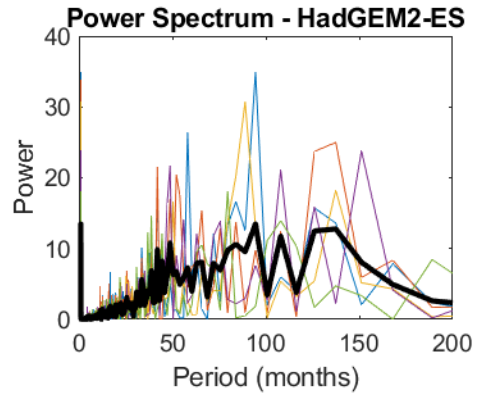
Power Spectrum - HadGEM2-ES
Power
Period (months)
0
10
20
30
40
0
50
100
150
200

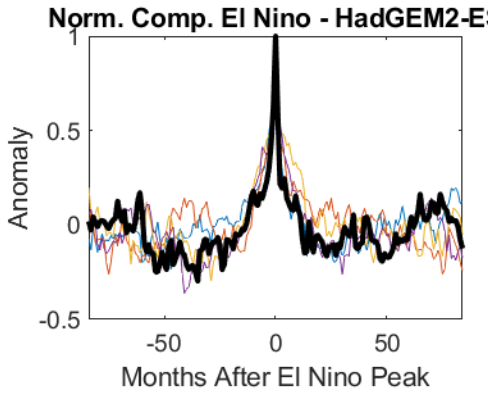
Norm. Comp. El Nino - HadGEM2-ES
Anomaly
Months After El Nino Peak
-0.5
0
0.5
1
-50
0
50

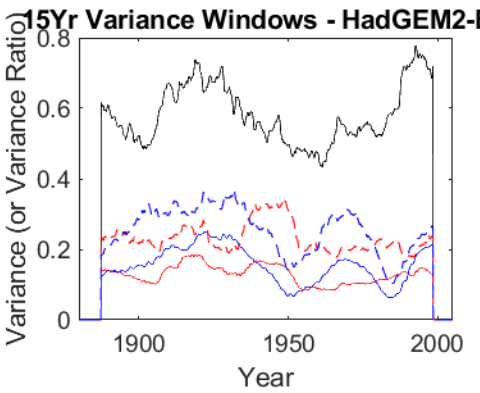
15Yr Variance Windows - HadGEM2-ES
Variance (or Variance Ratio)
Year
0
0.2
0.4
0.6
0.8
1900
1950
2000

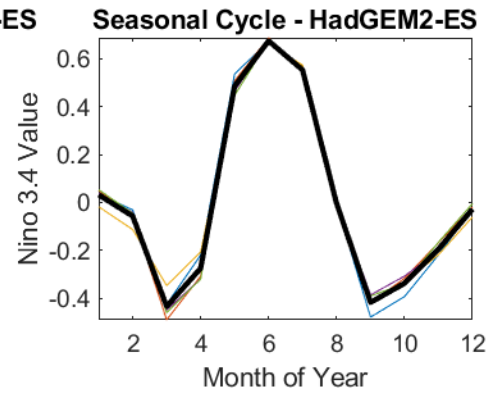
Seasonal Cycle - HadGEM2-ES
Nino 3.4 Value
Month of Year
-0.4
-0.2
0
0.2
0.4
0.6
2
4
6
8
10
12

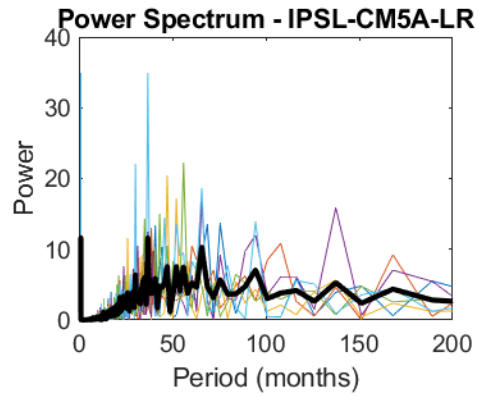
Power Spectrum - IPSL-CM5A-LR
Power
Period (months)
0
10
20
30
40
0
50
100
150
200

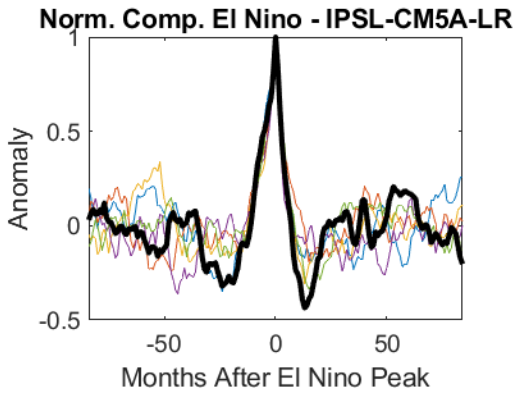
Norm. Comp. El Nino - IPSL-CM5A-LR
Anomaly
Months After El Nino Peak
-0.5
0
0.5
1
-50
0
50

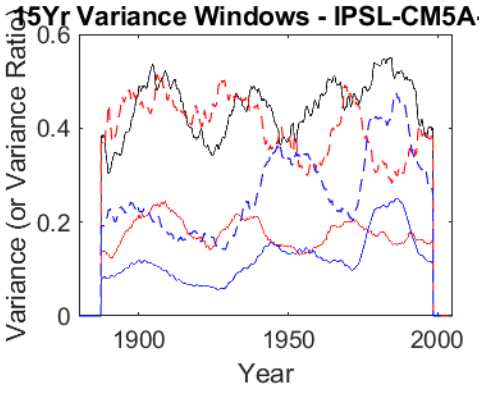
15Yr Variance Windows - IPSL-CM5A-LR
Variance (or Variance Ratio)
Year
0
0.2
0.4
0.6
1900
1950
2000

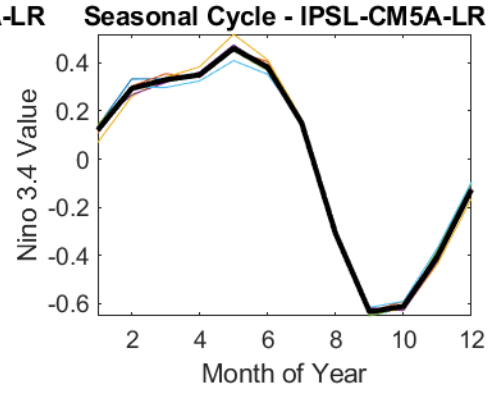
Seasonal Cycle - IPSL-CM5A-LR
Nino 3.4 Value
Month of Year
-0.6
-0.4
-0.2
0
0.2
0.4
2
4
6
8
10
12

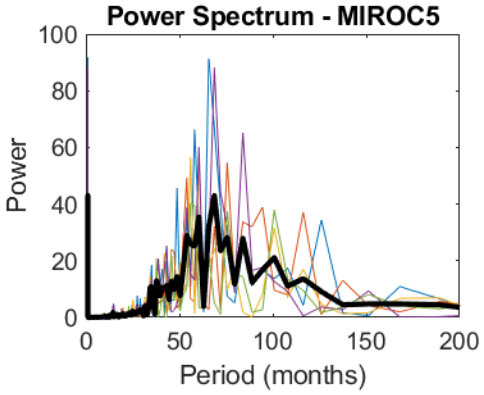
Power Spectrum - MIROC5
Power
Period (months)
0
20
40
60
80
100
0
50
100
150
200

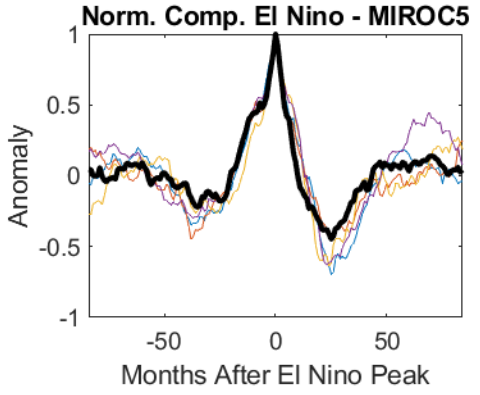
Norm. Comp. El Nino - MIROC5
Anomaly
Months After El Nino Peak
-1
-0.5
0
0.5
1
-50
0
50

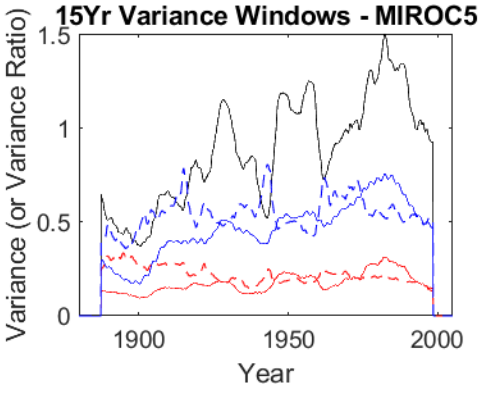
15Yr Variance Windows - MIROC5
Variance (or Variance Ratio)
Year
0
0.5
1
1.5
1900
1950
2000

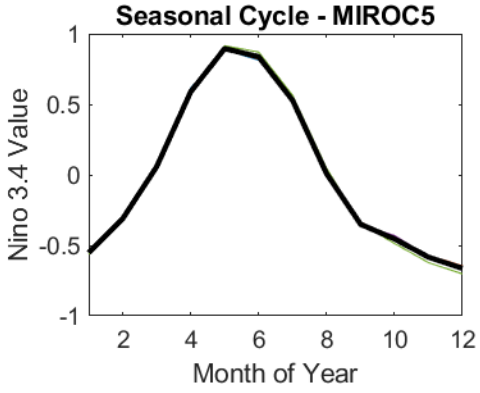
Seasonal Cycle - MIROC5
Nino 3.4 Value
Month of Year
-1
-0.5
0
0.5
1
2
4
6
8
10
12

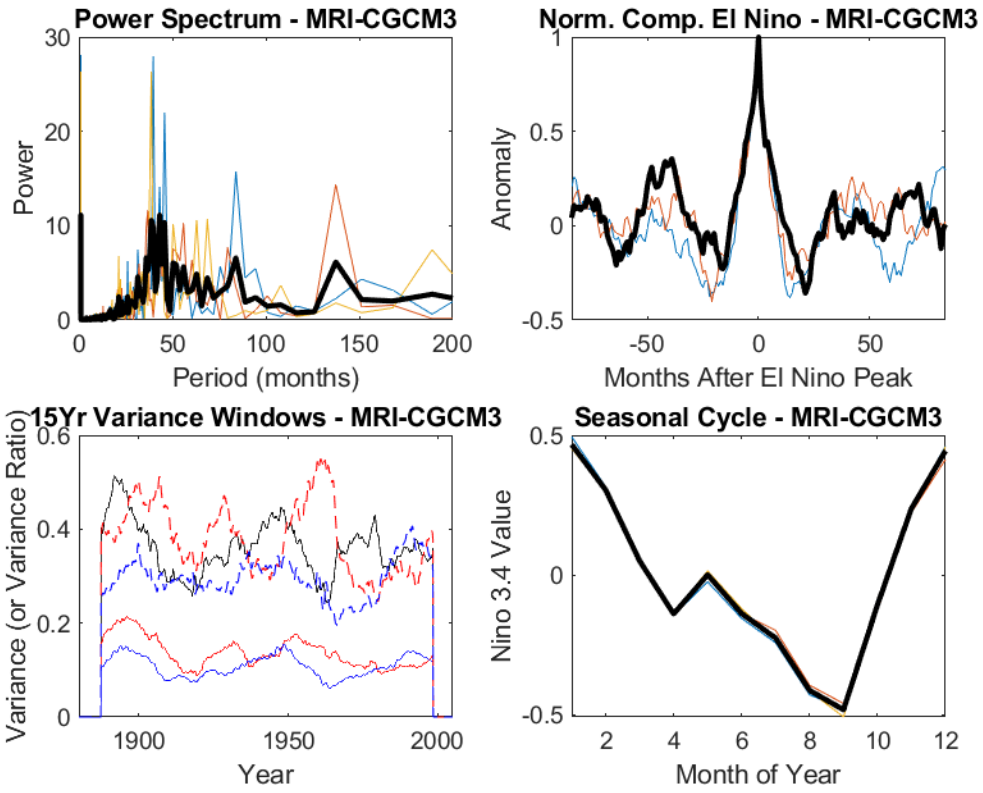
Power Spectrum - MRI-CGCM3
Power
Period (months)
Norm. Comp. El Nino - MRI-CGCM3
Anomaly
Months After El Nino Peak
15Yr Variance Windows - MRI-CGCM3
Variance (or Variance Ratio)
Year
Seasonal Cycle - MRI-CGCM3
Nino 3.4 Value
Month of Year